JOC The Journal of Organic Chemistry

Article

pubs.acs.org/joc

Benzimidazole-Branched Isomeric Dyes: Effect of Molecular Constitution on Photophysical, Electrochemical, and Photovoltaic Properties

Govardhana Babu Bodedla,[†] K. R. Justin Thomas,*[,†] Miao-Syuan Fan,[‡] and Kuo-Chuan Ho[‡]

[†]Organic Materials Chemistry, Department of Chemistry, Indian Institute of Technology Roorkee, Roorkee-247 667, India

[‡]Department of Chemical Engineering, National Taiwan University, Taipei 10617, Taiwan

Supporting Information

ABSTRACT: Three benzimidazole-based isomeric organic dyes possessing two triphenylamine donors and a cyanoacrylic acid acceptor are prepared by stoichiometrically controlled Stille or Suzuki–Miyaura coupling reaction which predominantly occurs on the *N*-butyl side of benzimidazole due to electronic preferences. Combined with the steric effect of the *N*-butyl substituent, placement of the acceptor segment at various nuclear positions of benzimidazole such as C2, C4, and C7 led to remarkable variations in intramolecular charge transfer absorption, electron injection efficiency, and charge recombination kinetics. The substitution of acceptor on the C4 led to red-shifted absorption, while that on C7 retarded the charge transfer due to twisting in the structure caused by the butyl group. Because of the cross-conjugation nature and poor electronic interaction between the donor and acceptor, the dye containing triphenylamine units on C4 and C7 and the acceptor unit on C2 showed the low oxidation potential. Thus, this dye possesses favorable HOMO and LUMO energy levels to render efficient sensitizing action in solar cells. Consequently, it results in high power conversion efficiency (5.01%) in the series with high photocurrent density and open circuit voltage. The high photocurrent generation by this dye is reasoned to it exceptional charge collection efficiency as determined from the electron impedance spectroscopy.

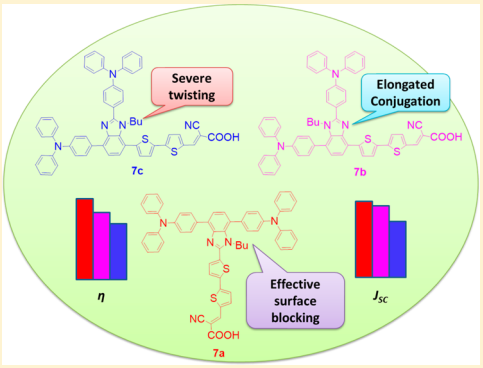

INTRODUCTION

Day to day increase in demand for energy and depletion of natural sources such as fossil fuels necessitate the need for alternative renewable energy sources. Though silicon-based solar cells suffice the demand partly, they suffer due to cost and cumbersome fabrication procedures. Organic solar cells (OSCs), particularly, dye-sensitized solar cells (DSSCs) invented by Grätzel et al.[1] are attractive and fill the gap. A large variety of DSSCs have been demonstrated employing Ru(II)-polypyridyl-,[2] porphyrin-,[3] phthalocyanin-,[4] perovskite-,[5] and organic dyes[2a,6] as sensitizers and achieved efficiency as high as >15%.[7] Each category of dyes inherit their own advantages and disadvantages as sensitizers. Despite this, organic dyes featuring D-π-A molecular configuration have shown potential due to their low cost of production, ready availability, high molar extinction coefficients for intramolecular charge transfer (ICT) bands, environmental friendliness, and structural response toward optical and photovoltaic properties.[2a,8] Organic dyes have been demonstrated to exhibit power conversion efficiency >10–12.8%.[9]

Efficiency of DSSC is often hampered by the poor driving force for electron injection and dye regeneration and recombination of injected electrons with the oxidized dye or electrolyte components.[2−9] These detrimental processes affect the short circuit photocurrent (J_{SC}) and open circuit voltage (V_{OC}) directly. Recent attempts on dye design have mainly focused on optimizing these parameters by structural engineering. The J_{SC} can be enhanced by the following strategies: (a) Extension of the ICT absorption in the dyes into the lower energy region with high molar extinction coefficients by either linking or inserting suitable donors, linkers, and acceptors in D-π-A configuration of organic dyes.[10] (2) Incorporation of two or more D-π-A segments in a single molecule may effectively populate the number of light-harvesting D-π-A units on the surface of TiO_2.[11] (3) Co-sensitization of complementary organic dyes also lead to a broad coverage of solar light and thus broader IPCE spectra and enhanced J_{SC}.[9a,12] The V_{OC} is generally improved by the following methods: (1) excluding the $\pi-\pi$ stacking interaction of sensitizers on the surface of nanocrystalline TiO_2 film by employing bulky donor moieties,[10,13] with the incorporation of either twisted π-linkers[10b,14] or alkoxy and alkyl groups on donor and linker parts of D-π-A dyes.[10,15] (2) Facile dye regeneration by lowering the HOMO energy level of the dye has been proven to increase the V_{OC} by reducing the charge recombination between the oxidized sensitizer and conduction band (E_{cb}) of

Received: November 10, 2015
Published: December 17, 2015

DOI: 10.1021/acs.joc.5b02590
J. Org. Chem. 2016, 81, 640–653

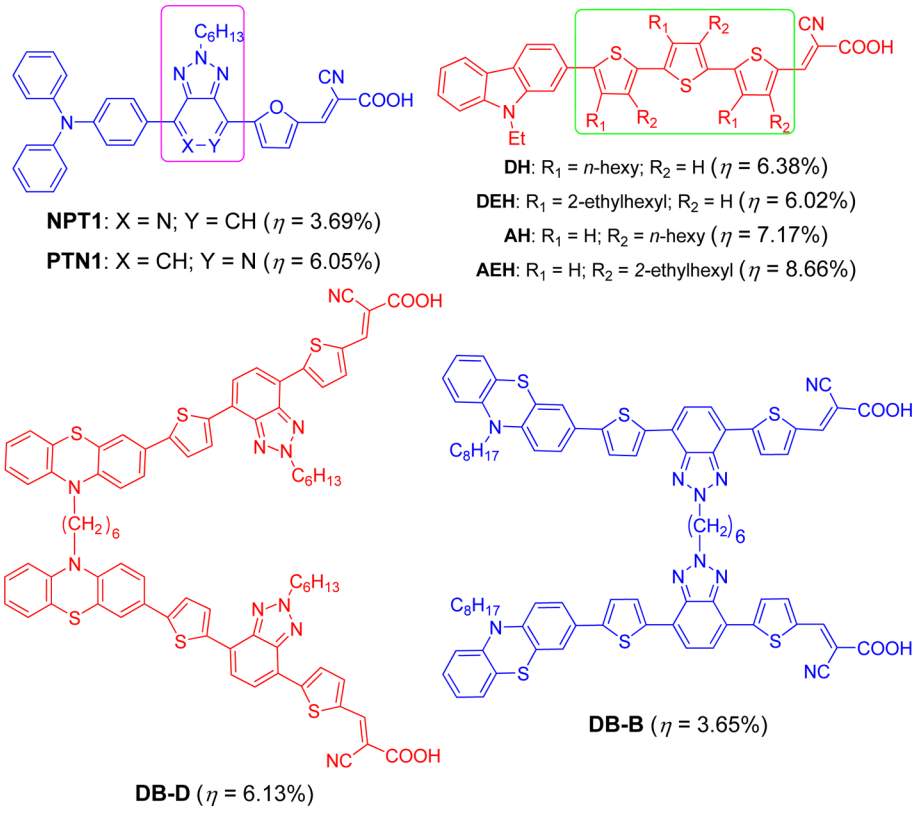

Figure 1. Isomeric organic dyes known in the literature.

TiO_2.[12c,13a,16] (3) Replacing the conventional iodine-based electrolyte with $Co^{(II)/(III)}$ tris(bipyridyl)-based redox electrolyte (0.5 V vs NHE)[17,18] and Br_3^-/Br^- redox electrolytes (1.1 V vs NHE)[19] have been demonstrated to increase the potential barrier between the conduction band energy (E_{cb}) of TiO_2 and redox electrolytes. This efficiently jeopardizes the dark current and enhances V_{OC}. (4) Finally, the addition of an optimum amount of coadsorbents such as chenodeoxycholic acid (CDCA) also increases the V_{OC} of DSSC by reducing the aggregation of dye molecules.[20]

Isomeric dyes with difference in constitution have received immense attention recently due to the tunability of optical and photovoltaic properties while maintaining the structural components. Lin and co-workers[21] synthesized two isomeric sensitizers **NPT1** and **PTN1** (Figure 1) containing a 2*H*-[1,2,3]triazolo[4,5-*c*]pyridine auxiliary acceptor. The dye with pyridine nitrogen on the donor side (**NPT1**) exhibited high efficiency (6.06%) than the isomeric dye containing pyridine nitrogen facing the acceptor side (**PTN1**, η = 3.69%). The dye **NPT1** showed intense absorption and high oxidation potential indicative of the effective charge transfer due to the proximity of the electronegative nitrogen to the donor. Wang and co-workers[22] reported isomeric dyes which possessed variation in the position of alkyl substituents on the linker. The dyes **AH** and **AEH** featuring alkyl groups in the direction of acceptor exhibited better performance than the dyes **DH** and **DEH** containing alkyl groups on the donor side. Former dyes showed high J_{SC} attributable to the longer wavelength absorption with high molar extinction coefficients, while the later dyes gave rise to slightly high V_{OC} values arising from the twisted structures which effectively suppressed the electron recombination and increased the electron lifetime. Huang et al.[23] synthesized two isomeric double branched D-π-A organic dyes differing in the linkage position between the D-π-A chromophores. Despite possessing similar optical and electrochemical properties, the DSSC based on the dye **DB-D** which contains the linkage between the donor units displayed higher overall power conversion efficiency (6.13%) than the dye **DB-B** with the connection at the π-bridge (3.65%). The better efficiency of **DB-D** is attributed to its reduced aggregation and effective surface blocking. In addition to these reports, a few isomeric dyes were well documented in the literature.[24]

Recently, benzimidazole[25] and imidazole[26] motifs have attracted extensive attention as auxiliary donors and bulky hydrophobic moieties in organic dyes, and such dyes demonstrated improved light-harvesting properties and reduced charge recombination rates. In our earlier report,[27] we have shown that *N*-phenylbenzimidazole incorporated phenothiazine based dyes exhibited red-shifted absorption and hence high J_{SC}, jeopardized unwanted charge recombination, and enhanced V_{OC}. As a result, the DSSC devices sensitized with *N*-phenylbenzimidazole bearing phenothiazine dyes exhibited high efficiency when compared to that of the control dye. Herein, we report the synthesis and characterization of three isomeric dyes (Figure 2) containing *N*-butylbenzimidazole as a branch, two triphenylamine donors, and a bithiophene cyanoacrylic acid acceptor segment. The dyes were synthesized by selective Suzuki or Stille coupling reactions followed by Knoevenagel condensation. The dyes showed variations in the attachment of the acceptor segment in the benzimidazole nucleus. The presence of the acceptor segment on C2 (**7a**) and C7 (**7c**) of the benzimidazole nucleus led to drastic decrement in the propensity of the ICT and produced blue-shifted absorption. However, the dye **7a** led to better overall power conversion efficiency in the DSSC due to the effective inhibition of the recombination of electrons and facile injection of electrons into the conduction band to

DOI: 10.1021/acs.joc.5b02590
J. Org. Chem. 2016, 81, 640−653

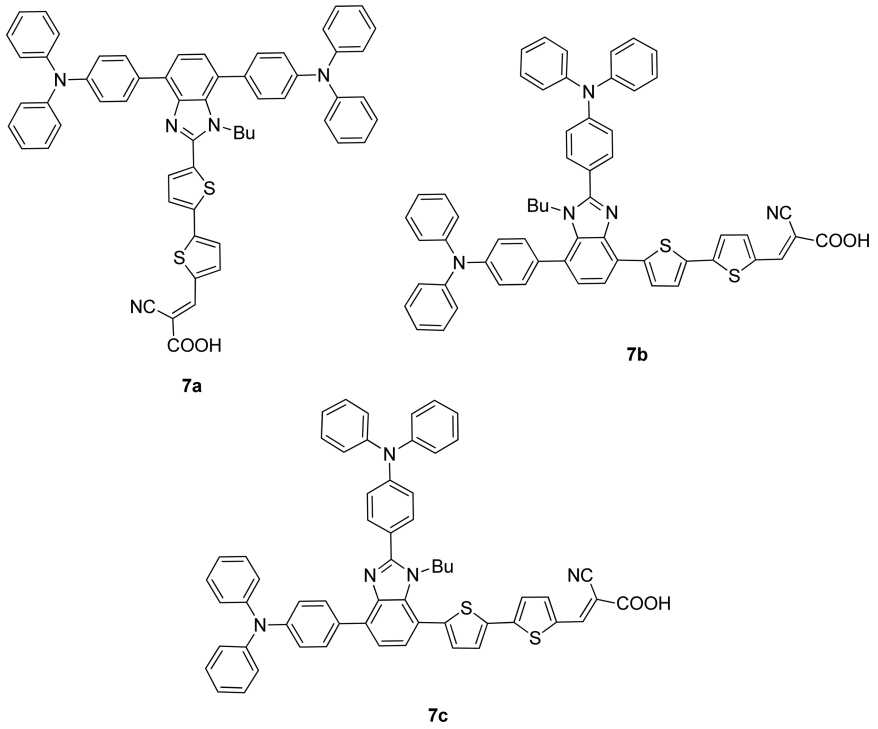

Figure 2. Structures of benzimidazole-based isomeric dyes used in this study.

Scheme 1. Synthesis of the Dye 7a

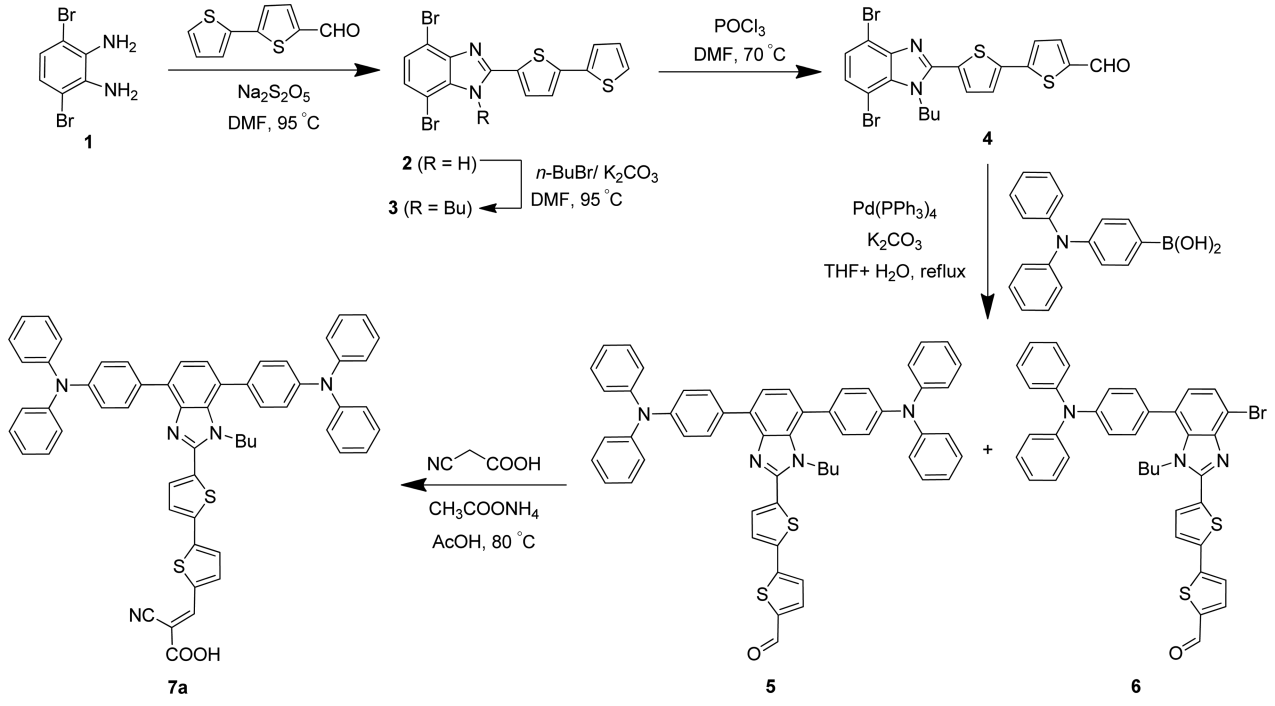

TiO_2. Although cross-conjugated organic fluorophores displaying acidochromism have been reported based on 2,4,7-trisubstituted benzimidazole,[28] to the best of our knowledge organic sensitizers are not reported.

RESULTS AND DISCUSSION

Synthesis and Characterization. The dyes were synthesized by following the protocols illustrated in Schemes 1−3. First, 2-aryl substituted 3,4-dibromo-1-butyl-1*H*-benzo[*d*]imidazoles (**3** and **9**) required for the work were synthesized by a two-step sequence. The reaction of 3,6-dibromobenzene-1,2-diamine (**1**) with 2,2′-bithiophene-5-carbaldehyde or 4-formyltriphenylamine in the presence of sodium metabisulfite ($Na_2S_2O_5$) in dimethyl formamide (DMF)[29] produced the corresponding 2-aryl-3,4-dibromo-1*H*-benzo[*d*]imidazoles, **2** and **8** (Schemes 1 and 2). They were N-alkylated using 1-bromobutane and K_2CO_3 in DMF[30] to obtain the N-butylated derivatives, **3** and **9**. For the synthesis of **7a**, dibromide **3** was subjected to formylation with

DOI: 10.1021/acs.joc.5b02590
J. Org. Chem. 2016, 81, 640−653

Scheme 2. Synthesis of the Dye 7b

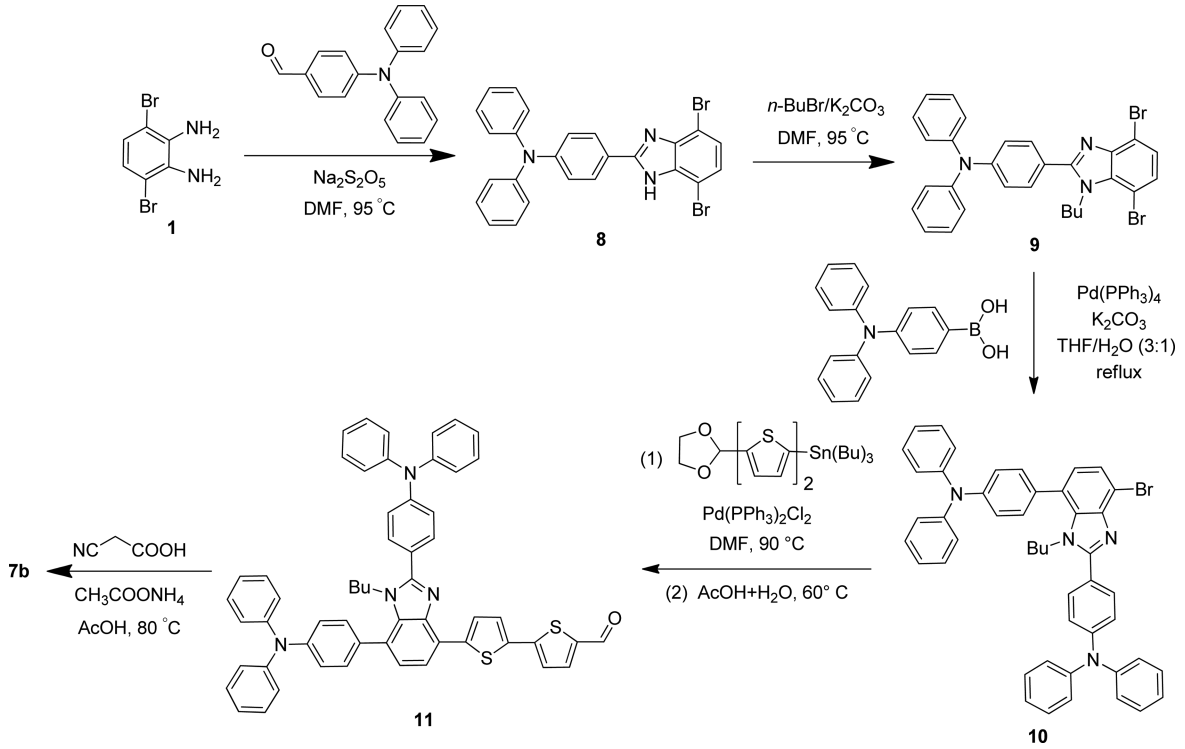

$POCl_3$/DMF to obtain the aldehyde derivative, **4**. Compound **4** was treated with 4-(diphenylamino)phenylboronic acid under Suzuki–Miyaura conditions[31] to obtain both mono- and dicoupled products, **6** and **5**.

The isolation of monocoupled product **6** gave evidence for the substitution pattern. Since the C4 and C7 positions of *N*-butyl-1-*H*-benzo[*d*]imidazole are chemically different, the aryl group can be delivered at either of these positions in the Suzuki coupling reaction. Though C7 is sterically hindered due to the butyl group, the first substitution occurs at this position due to the electronic preference (Scheme 3). The nitrogen lone pair electrons may be dissipated toward C4 or C7 due to the inductive electron withdrawal by electronegative bromine. The lone pair movement toward C4 is viable as it leads to more favored charge separated species. This was also confirmed by the Mulliken charge estimation. Accumulation of charge at C4 will hinder the oxidative addition step in the Suzuki coupling reaction and thus preferentially produce the C7-substituted product. The structure of **6** was established by single crystal X-ray analysis which confirms the location of the triphenylamine donor at C7 (Figure S37). The disubstituted aldehyde **5** was converted to the desired dye **7a** on treatment with cyanoacetic acid in acetic acid in the presence of ammonium acetate.[32]

Similarly, compound **9** was subjected to a stoichiometrically controlled Suzuki coupling reaction to obtain benzimidazole derivative **10** containing two donors and a bromine exclusively at C4 (Scheme 2). This was further converted to aldehyde derivative **11** by a Stille coupling[33] reaction with (5′-(1,3-dioxolan-2-yl)-[2,2′-bithiophen]-5-yl)tributylstannane followed by acid hydrolysis. Reaction of this aldehyde with cyanoacetic acid produced the dye **7b**. In a similar way starting from **9**, but reversing the reaction sequence (Scheme 4), i.e., the Stille coupling reaction of (5′-(1,3-dioxolan-2-yl)-[2,2′-bithiophen]-5-yl)tributylstannane followed by Suzuki coupling with 4-(diphenylamino)phenylboronic acid, the isomeric aldehyde

Scheme 3. Role of Nitrogen Lone Pair Electrons and Charge Accumulation at C4 and C7

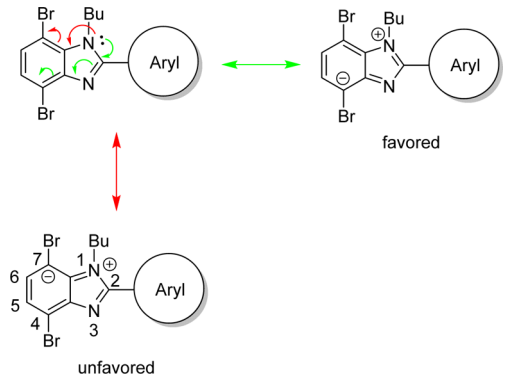

13 was obtained in modest yield. Condensation of **13** with cyanoacetic acid produced the third isomeric dye **7c**. All of the new compounds were thoroughly analyzed by IR, NMR (^{1}H and ^{13}C), and high resolution mass spectrometry. The spectral data are consistent with the proposed structures. All dyes are fairly soluble in tetrahydrofuran (THF), DMF, and chlorinated solvents such as dichloromethane and chloroform. However, they displayed poor solubility in toluene, alcohols, etc.

Optical Properties. The absorption spectra of the dyes recorded in THF (Figure 3a) displayed a broad envelope-like structure with three distinguishable peaks. The highest energy band at ca. 300 nm is probably originating from the triphenylamine localized $\pi-\pi^*$ excitation.[21] The middle and longest wavelength absorptions of the dyes show variations attributable to the structural changes in the dyes. First, the absorption maxima of the longest wavelength absorption of the dyes assume the order, **7b** > **7a** > **7c**. The reverse trend is witnessed for the middle wavelength absorption. The middle

DOI: 10.1021/acs.joc.5b02590
J. Org. Chem. 2016, 81, 640–653

Scheme 4. Synthesis of the Dye 7c

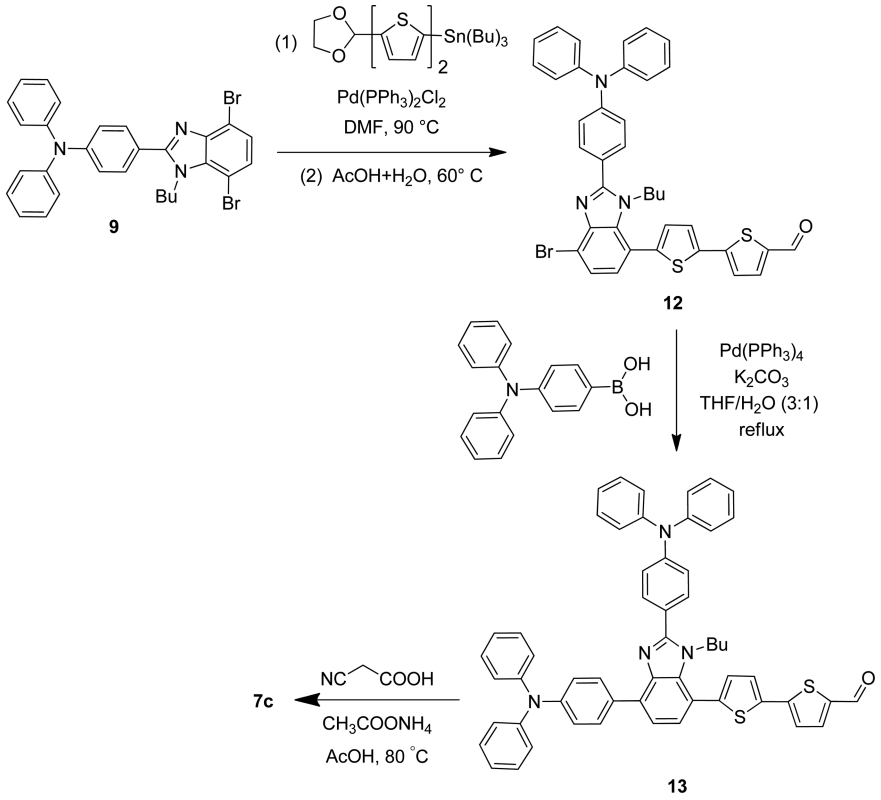

wavelength absorption is attributed to the $\pi-\pi^*$ transition originating from the bithiophene and cyanoacrylic acid segment. The extension of conjugative delocalization of the benzimidazole and other neighboring units into this chromophore dictates the wavelength and molar extinction coefficient of this absorption. On comparing with the aldehydes **4**, **6**, and **12** (SI), slightly blue-shifted $\pi-\pi^*$ absorption is observed for the dyes **7a** and **7b**, while the peak position remains unaltered for **7c**. It is interesting to note that the geometrical position of the bithiophene segment in **7c** is similar to **12**, while in **7a** it is derived from **6**. However, the aldehydes **4** and **6** exhibited red-shifted absorption when compared to that of **12**. So the $\pi-\pi^*$ absorption in dye **7a** is expected to appear at a longer wavelength than that of **7c**. Contrary to this belief, **7c** showed red-shifted $\pi-\pi^*$ absorption. It can be rationalized as follows: (a) in **12**, the conjugation is restricted within bithiophene aldehyde as the butyl group twists the benzimidazole and bithiophene units. However, in **4** and **6** the conjugation is extended into benzimidazole from bithiophene. Thus, **4** and **6** show red-shifted absorption when compared to that of **12**. In the dyes, **7c** showed no change when compared to **12**, but the $\pi-\pi^*$ absorptions of **7a** and **7b** are blue-shifted when compared to that of **4** or **6**. It is probable that the introduction of an additional triphenylamine unit on **6** on C4 distorts the planarity between the benzimidazole and bithiophene (see theoretical calculations below) and reduces the conjugation length of the chromophore responsible for the $\pi-\pi^*$ absorption. The absence of changes between **4** and **6** further supports the steric role of the butyl group.

The longest wavelength absorption is predominantly attributed to the intramolecular charge transfer (ICT) between the triarylamine donor and cyanoacrylic acid acceptor.[6,8,9] The ICT peak positions of the dyes assumes the order: **7b** > **7a** > **7c**. The trend is intriguing when comparing the structural features of the dyes. Dye **7a** is cross-conjugated with a poor electronic communication between the donor and acceptor units. The dyes **7b** and **7c** contain a tilted donor–acceptor axis arising from the steric demand from the butyl group. It is interesting that the butyl group on the acceptor side in **7c** significantly affects the communication between the donor and acceptor when compared to the butyl group on the donor side in **7b**. It is also noteworthy that the steric effect due to the butyl group in **7c** significantly hampers the electronic delocalization than the cross-conjugation in **7a**. These perturbations manifested in the transition probability of ICT in these dyes. Thus, dye **7b** displayed the highest molar extinction coefficient in the series followed by **7a** and **7c** in that order. Nevertheless, all the dyes exhibited molar extinction coefficients larger than that of the popularly used ruthenium dyes **N8** and **N719**. To summarize, the optical data clearly establish the importance of the coplanar arrangement of the acceptor with the linker, in this case benzimidazole, than the donor.

The absorption spectra of the dyes anchored on porous nanocrystalline TiO_2 films are shown in Figure 3b. All of the dyes displayed a red-shifted absorption edge compared to that observed in tetrahydrofuran solution (Figure 3a). The bathochromic shift and broadening are more drastic for dye **7a**. Generally, the red shift is attributed to the formation of *J*-type aggregates[34] of the dye molecules or due to the large thickness of the TiO_2 layer.[35] In the present dyes, the T-shaped molecular configuration and the presence of two trigonal triphenylamine units would help to retard the formation of aggregates (see below). So, the observed broadening and red-shift may be ascribed mainly to the large thickness of the TiO_2 layer. However, the unusual red shift for **7a** points to the fact that the angular arrangement of the triphenylamine units in **7b** and **7c** effectively

DOI: 10.1021/acs.joc.5b02590
J. Org. Chem. 2016, 81, 640–653

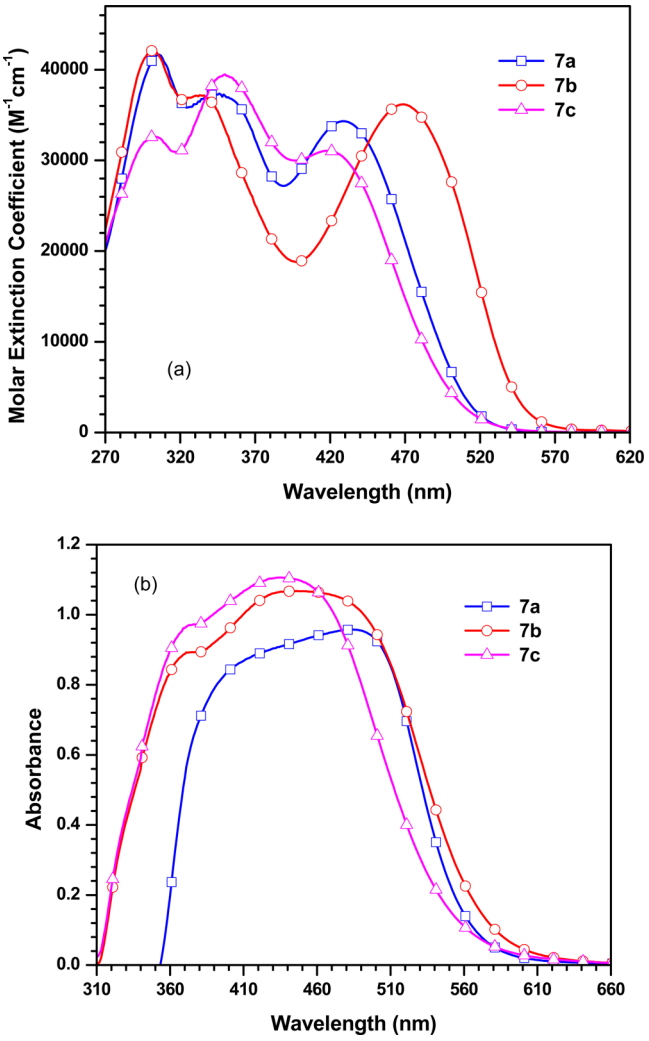

Figure 3. Absorption spectra of the dyes recorded in (a) tetrahydrofuran solution and (b) anchored on nanocrystalline TiO_2.

inhibits the aggregation when compared to the linear arrangement of triphenylamines units in **7a**.

The emission spectra of the dyes recorded in THF (Figure S38b) exhibited a trend similarly observed in absorption spectra. Dye **7b** exhibited the red-shifted emission peak when compared to those of **7a** and **7c**, but the Stokes shift of **7b** is the smallest among the dyes. This indicates that dye **7b** undergoes lower structural reorganization in the excited state when compared to that of **7a** and **7c**. This is reasonable as dye **7b** is more planar when compared to dyes **7a** and **7c** (vide supra). This is in accordance with the very high Stokes shifts reported for the dyes having a twisted structure than the isomeric molecules with planar configuration.[22] When the emission spectra of the dyes were measured in nonpolar solvent such as toluene, a reverse trend was observed (Figure S38a). Dye **7b** exhibited the most blue-shifted emission profile in the series. This further supports our argument that **7b** possesses more polarized structure in the series arising from the strong ICT character. Such polar molecules will be effectively solvated by the polar solvents, while the nonpolar solvents cannot.

The effect of the solvent polarity on the ICT absorption peak of the dyes were examined by recording the absorption spectra of the dyes in different solvents such as toluene (TOL), dichloromethane (DCM), tetrahydrofuran (THF), methanol (MeOH), acetonitrile (ACN), and dimethylformamide (DMF). All the dyes exhibited a blue shift for ICT absorption on increasing the solvent polarity indicating appreciable donor−acceptor interaction in the ground state (see for instance, Figure 4). Most

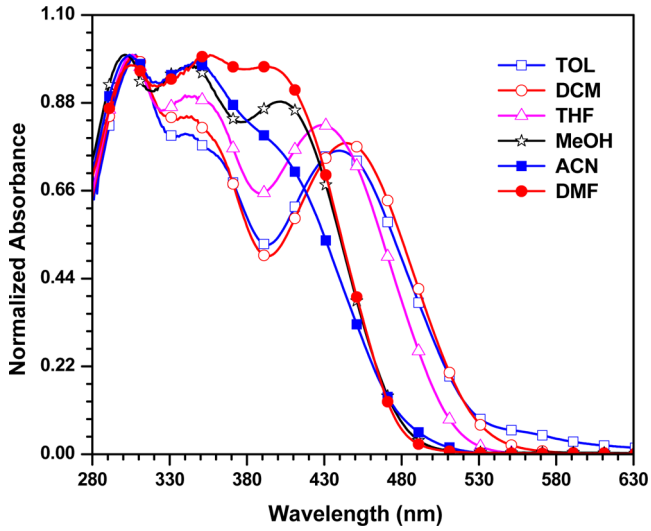

Figure 4. Absorption spectra of **7a** recorded in different solvents.

red-shifted absorption was observed for DCM probably arising from the instant stabilization of polarizable electrons.[36] Most blue-shifted absorption witnessed for DMF, MeOH, and ACN solutions may be attributed to the effective solvation of the dyes by the polar solvents and to the basic nature of DMF.[37]

The ICT character of the longer wavelength absorption is further corroborated by the acid−base equilibria of the dyes (Figure 5). The dyes on addition of TEA displayed a significant

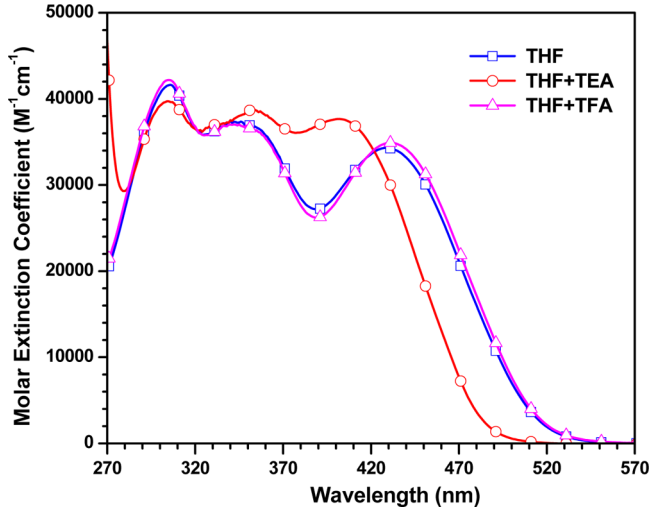

Figure 5. Absorption spectra of **7a** recorded in THF before and after the addition of TFA or TEA.

blue shift for the charge transfer band. However, the addition of TFA did not alter the absorption. This clearly points that the dyes are in the protonated form in solution.[38,39] However, the hypsochromic shifts upon addition of the base are rather limited which highlight the existence of charge transfer between the cyano moiety and the donor part of the chromophore.

DOI: 10.1021/acs.joc.5b02590
J. Org. Chem. 2016, 81, 640−653

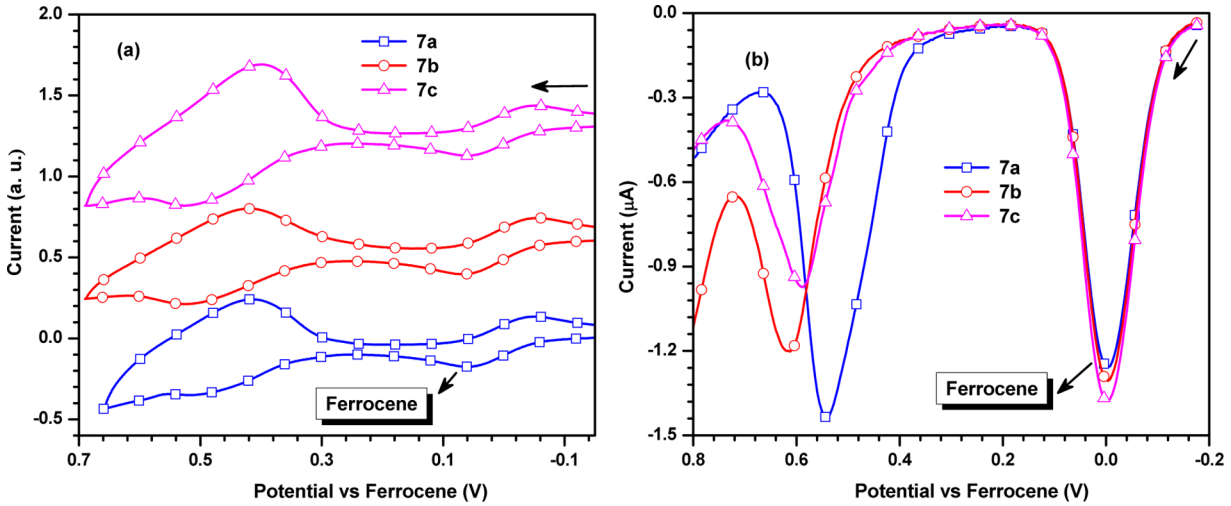

Figure 6. (a) Cyclic voltammograms and (b) differential pulse voltammograms of the dyes recorded for tetrahydrofuran solutions.

Table 1. Photophysical and Electrochemical Properties of Dyes in Tetrahydrofuran Solution

dye	λ_{abs} (nm) ($\varepsilon_{max} \times 10^3$ M^{-1} cm^{-1})	λ_{em} (nm)	Stokes shift (cm^{-1})	E_{ox} (mV) (ΔEp (mV))[a]	E_{ox} (eV) (vs NHE)[a]	E^*_{ox} (eV)[b] (vs NHE)	HOMO[c] (eV)	LUMO[d] (eV)	E_{0-0}[e] (eV)	ΔG_{inj}[f]
7a	428 (34.33), 346 (37.36), 306 (41.64)	562	5571	544 (82)	1.31	−1.22	5.34	2.81	2.53	−0.72
7b	469 (36.18), 333 (37.18), 302 (42.15)	577	3991	616 (85)	1.39	−0.97	5.42	3.06	2.36	−0.47
7c	418 (31.06), 350 (39.47), 303 (32.62)	562	6130	588 (89)	1.36	−1.21	5.39	2.82	2.57	−0.71

[a] E_{ox} (vs NHE) = 0.77 + E_{ox} (vs Fc). Oxidation potential of the dyes were recorded in THF (2×10^{-4} M) with 0.1 M Bu_4NClO_4 as electrolyte (working electrode, glassy carbon; counter electrode, Pt wire; reference electrode, nonaqueous Ag/Ag^+; ferrocene was used as internal standard for potential calibration). [b] Calculated using the formula $E^*_{ox} = E_{ox} - E_{0-0}$. [c] Obtained from the oxidation potential using the formula HOMO = 4.8 + E_{ox}. [d] Calculated using the formula LUMO = HOMO − E_{0-0}. [e] Estimated from the intersection between the normalized absorption and emission spectra. [f] Thermodynamic driving force of the electron injection (ΔG_{inj}) = $E^*_{ox} - E_{CB}$.

Electrochemical Characteristics. Electron injection from the photoexcited dye into the conduction band of TiO_2 and the regeneration of the oxidized dye by the electrolyte depends on excited and ground state oxidation potentials, respectively, of the dyes. The ground and excited state oxidation potentials of the dyes can be deduced from the redox potentials of the dyes and the optical band gap.[27] Thus, to ascertain the thermodynamic feasibility of electron injection and dye regeneration we had performed electrochemical studies on the dyes by using cyclic and differential pulse voltammetric techniques. The cyclic and differential pulse voltammograms of the dyes are displayed in Figure 6 and the corresponding redox parameters listed Table 1. All of the dyes displayed a broad redox couple attributable to the removal of two electrons simultaneously from the triphenylamine units. The oxidation potentials of the dyes are more positive than that of internal ferrocene. It is interesting that the two chemically different triphenylamine units in the dyes did not show distinguishable oxidation peaks. Nevertheless, the oxidation potentials of the dyes exhibited a trend (**7b** > **7c** > **7a**) reflecting the strength of interaction between the donor and acceptor. The lowest oxidation potential observed for **7a** is due to the completely delinked T-shaped structure, which isolates the triphenylamine units from the acceptor segment. However, in the case of **7b** and **7c** the triphenylamine unit is directly linked to the acceptor in a linear conjugation. However, the conjugation between the donor and acceptor is affected by the nonplanarity originating from the steric inhibition rendered by *N*-butyl group. It has been already established from the absorption data that the interaction between the donor and acceptor in **7b** is better than that in **7c**. The relatively high oxidation potential observed for **7b** over **7a** further supports this.

The ground state oxidation potentials (E_{ox}) corresponding to HOMO energy levels and the excited state oxidation potentials (E^*_{ox}) corresponding to LUMO energy levels of the dyes fall in the range 1.31−1.36 V and −0.97 V to −1.22 V (vs. NHE), respectively. Furthermore, the E_{ox} values are more positive (Figure 7) than the redox potential of iodine/iodide (I_3^-/I^-)

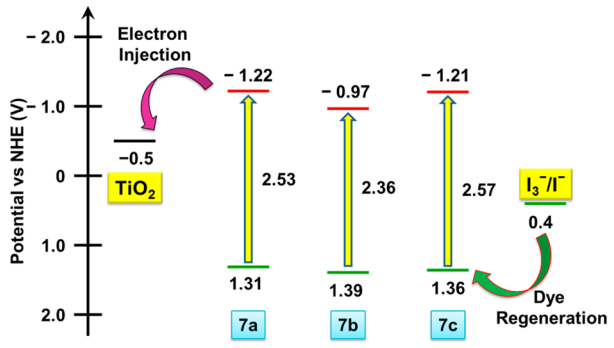

Figure 7. Ground state and excited state oxidation potentials of the dyes with respect to NHE.

electrolyte (0.4 V vs. NHE),[8b,c,40] while the E^*_{ox} values are more negative (Figure 7) than the E_{cb} of TiO_2 (−0.5 V vs. NHE).[8b,c,41] This suggests a favorable thermodynamic driving force for the regeneration of the oxidized dyes by electrolyte and effective

DOI: 10.1021/acs.joc.5b02590
J. Org. Chem. 2016, 81, 640−653

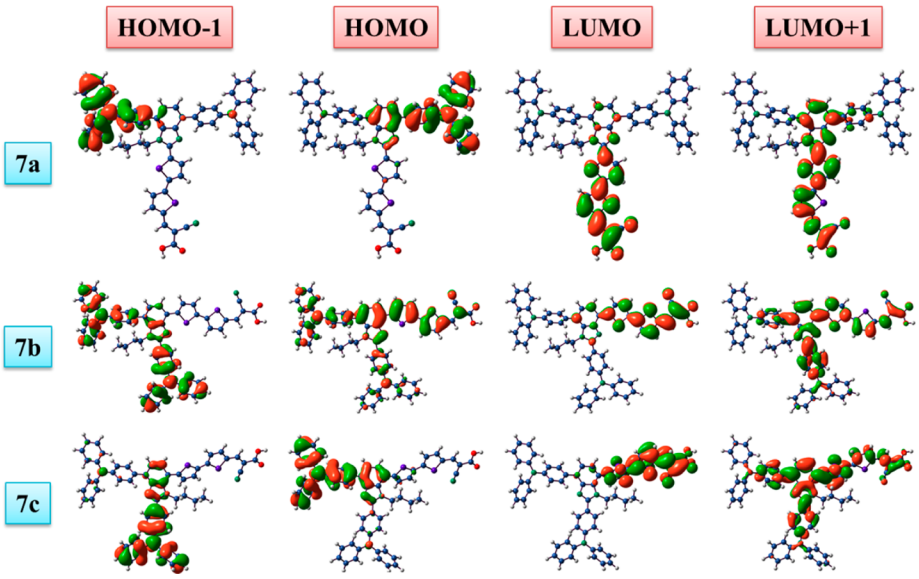

Figure 8. Calculated electronic distribution in frontier molecular orbitals of the dyes.

Table 2. Computed Vertical Transitions and Their Oscillator Strengths and Configurations Using the MPW1*K*/6-31G(d,p) Level

dye	λ_{max} (nm)	f	configuration	HOMO (eV)	LUMO (eV)	E_{0-0} (eV)	μ_g (D)
7a	477	1.09	HOMO − 2→LUMO (39%), HOMO→LUMO (55%)	−5.89	−2.55	3.34	12.93
7b	489	1.67	HOMO − 2→LUMO (30%), HOMO→LUMO (62%)	−6.03	−2.40	3.63	17.12
7c	446	1.26	HOMO − 2→LUMO (37%), HOMO→LUMO (56%)	−5.90	−2.43	3.47	5.78

injection of electrons from the photoexcited dye into the CB edge of TiO_2, respectively. The dye **7a** possessed relatively high-lying E^*_{ox} value (Table 1) which may increase the thermodynamic driving force for electron injection (ΔG_{inj}) and consequently improve the electron collection efficiency in the DSSC.[9a]

Theoretical Investigations. The electronic structure of the dyes were analyzed by density functional theoretical (DFT)[42] calculations using the Gaussian 09 program package. In the present dyes, the *N*-butyl group plays a major role in the planarity of the molecule; the position of other groups relative to this is expected to exert a significant effect on the optical and electrochemical properties. It is worth studying the impact of geometrical arrangement on the organization of frontier molecular orbitals and the propensity of intramolecular charge transfer. Generally, the donor−acceptor interactions in the organic dyes mainly depend on the coplanarity of the consecutive chromophores, which dictates the conjugative communication between the constituents.[14c] The calculated interplanar angles between the various aromatic segments in the dyes are shown in Figure S39. As expected, the segment on the *N*-butyl side is significantly deviating from the planarity. The deviation is more significant when the chromophore on the *N*-butyl side is the triphenylamine unit (**7a** and **7b**). Also, the triphenylamine moiety on the other side of the benzimidazole also showed deviation from the planarity (compare **7a** and **7c** with **7b**) originating from the tilting of the phenyl group. However, the acceptor segment comprising bithiophene and cyanoacrylic acid displayed more coplanarity with the benzimidazole in **7b**. Thus, the donor−acceptor axis in **7c** is very distorted from the planarity, while in **7b**, the twisting is mainly between benzimidazole and triphenylamine units. The polarization in the molecule can be grossly estimated from the dipole moment values. Significant donor−acceptor interaction is expected to result in a more polarized molecule. In **7c**, the distortion of the acceptor unit from the benzimidazole unit severely delinks the donor and acceptor moieties. Thus, the donor−acceptor interaction in **7c** is expected to be very minimal. The trend in dipole moments [**7b** (17.12 D) > **7a** (12.93 D) > **7c** (5.78 D)] is in line with these speculations. These structural arrangements greatly influenced the electronic distribution in the frontier molecular orbitals.

The computed frontier molecular orbitals HOMO, HOMO − 1, LUMO, and LUMO + 1 of the dyes are shown in Figure 8. Vertical excitation energies, their oscillator strengths, and orbital contribution are listed in Table 2. In the dyes **7a** and **7c**, the HOMO is located on the triphenylamine unit attached at the C4 position and benzimidazole. However, in **7b** the HOMO is mainly constituted by the bithiophene and benzimidazole units with minor contribution from the triphenylamine units. This is probably because of the noncoplanar arrangement of triphenylamine units with the benzimidazole unit. Thus, the conjugation is limited to the benzimidazole and bithiophene units. The LUMO in all the dyes are restricted to the bithiophene and cyanoacrylic acid segment. The HOMO and LUMO are completely separated in the dyes **7a** and **7c**, which reduces the propensity of charge transfer between the donor and acceptor. However, in **7b** due to the delocalization of HOMO over the entire molecule, the HOMO to LUMO excitation can be termed as a composite of $\pi-\pi^*$ and ICT. On this basis, a blue-shifted absorption is expected for **7a** and **7c** when compared to that of **7b**. Computed vertical transition and their orbital contributions are listed in Table 2. It is mainly contributed by the HOMO to LUMO and HOMO − 2 to LUMO electronic excitations. The order of theoretically calculated absorption maxima for the dyes is **7b** > **7a** > **7c**, and it is well matched with the absorption trend observed in THF solution (vide supra).

DOI: 10.1021/acs.joc.5b02590
J. Org. Chem. 2016, 81, 640−653

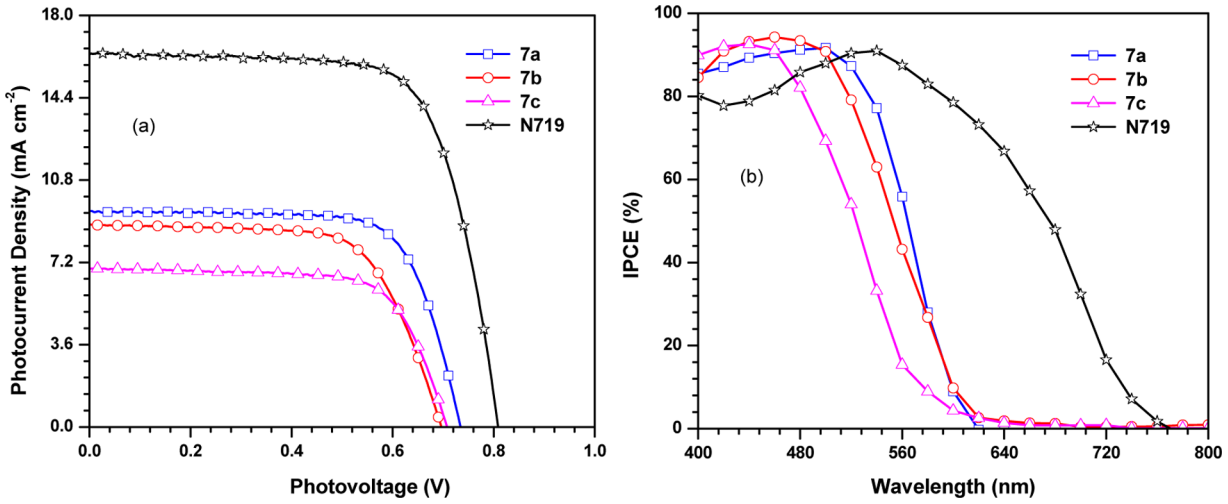

Figure 9. *I*–*V* curves (a) and IPCE spectra (b) of the DSSC fabricated using the *N*-butyl benzimidazole-based isomeric dyes.

Photovoltaic Properties. The photovoltaic properties of the dyes were evaluated by fabricating photoelectrochemical cells using the dyes as sensitizers. The short-circuit photocurrent vs open-circuit photovoltage (*J*–*V*) plots and incident photon-to-current conversion efficiency (IPCE) curves are shown in Figure 9 and relevant photovoltaic parameters compiled in Table 3. The dye **7a** exhibited the best performance (η = 5.01%) in the series, attributable to high photocurrent density (J_{SC}) and enhanced photovoltage (V_{OC}). The high photocurrent observed for **7a** is interesting. Particularly, the dye **7b** possesses comparatively better light-harvesting property than **7a**. So **7b** is expected to produce a larger photocurrent. Contrary to this belief, relatively low J_{SC} (8.84 mAcm^{-2}) was realized for **7b** probably due to the less favorable driving force for the electron injection into the conduction band of TiO_2 for the photoexcited dye originating from the low-lying LUMO. However, in **7a** the suitable position of LUMO increases the charge collection efficiency.

Table 3. Photovoltaic Performance Parameters of DSSCs Based on the Dyes

dye	J_{SC} (mA cm^{-2})	V_{OC} (V)	*ff*	η (%)	R_{rec} (Ω)	R_{ct2} (Ω)	τ_e (ms)
7a	9.42	0.73	0.72	5.01	63.12	15.32	4.54
7b	8.84	0.70	0.67	4.13	29.33	16.01	3.94
7c	6.92	0.71	0.71	3.45	38.78	17.88	3.94
N719	16.29	0.81	0.71	9.41	79.57	11.90	12.05

The relatively high V_{OC} for the dye **7a** may be attributed to the presence of two triphenylamine donor moieties at C4 and C7 positions of the benzimidazole core, which may provide effective surface blocking through steric hindrance to suppress the approach of the I_3^- species from the electrolyte toward TiO_2.[43] Similarly, a slight increase in V_{OC} for the dye **7c** when compared to its isomeric analogue **7b** may arise from the more twisted structure of the former (vide infra), which effectively blocks the phenomena responsible for charge recombination (vide supra). Similar observations were reported for the isomeric dye **DH**[22] possessing twisted π-linkers.[10b,14]

Electrochemical Impedance Spectroscopy (EIS). The trends in V_{OC} of the isomeric dyes can be evaluated by estimating the electron recombination resistance (R_{rec}) and electron transport resistance (R_{ct2}) in the devices across the TiO_2/dye/electrolyte interface, and also electron lifetime (τ_e) in the CB of TiO_2. In order to get these parameters, the Nyquist and

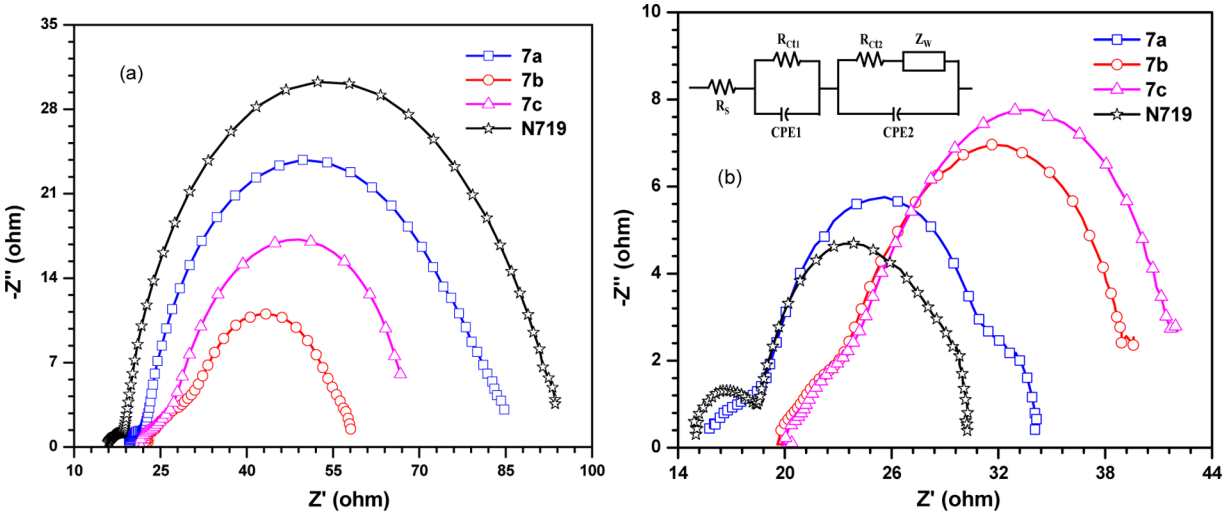

Figure 10. Nyquist plots of the DSSCs under (a) dark and (b) illumination conditions.

DOI: 10.1021/acs.joc.5b02590
J. Org. Chem. 2016, 81, 640–653

Bode-phase plots of DSSC devices were constructed by EIS measurements under dark and illumination conditions. The Nyquist plots of the devices under the dark and illumination conditions are shown in Figure 10, and the corresponding parameters listed in Table 3. The radius of the middle large semicircle in the Nyquist plots is related to the R_{rec} and R_{Ct2} under dark and illumination conditions, respectively.[2a,27,44,45] The order of R_{rec} of the dyes is **7a** > **7c** > **7b**, while the R_{ct2} assumes a trend **7c** > **7b** > **7a**. The high R_{rec} and low R_{ct2} observed for the device comprising **7a** is matching with the high J_{SC} and V_{OC} values. Further, the high V_{OC} for **7a** is supported by the relatively elongated electron lifetime deduced from the Bode phase plot (Figure11).[2a,27,44,45]To summarize, the best performance of **7a** with variations attributable to the isomeric constitution of the dyes. The T-shaped structural composition of **7a** was found to be beneficial for the retardation of electron recombination, while the isolation of donor and acceptor helped to upwardly shift the LUMO and increase the charge collection efficiency. Because of the high J_{SC} and V_{OC} values, the dye **7a** exhibited the highest efficiency (5.01%) among the isomeric dyes. These results indicate that benzimidazole is a versatile chromophore for the development of promising organic dyes by suitable position of donors, π-linkers, and acceptors on the benzimidazole nucleus.

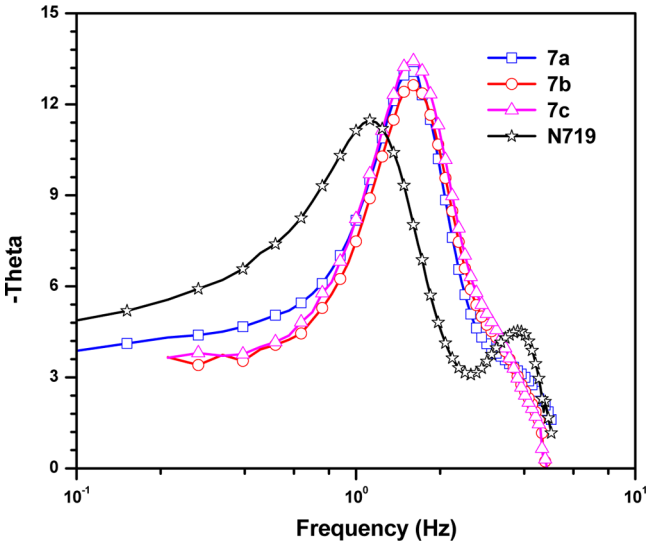

Figure 11. Bode phase plots of the DSSCs under illumination condition.

mainly originates from the high R_{rec}, τ_e, and low R_{ct2}. It also points to the fact that the integration of triphenylamine at C4 and C7 positions of benzimidazole is more desirable than the C2 and C7 and C2 and C4 positions to reduce the electron recombination between the injected electrons in the CB of TiO_2 with the oxidized dyes and redox constituents.[46]

CONCLUSIONS

We have designed and synthesized three benzimidazole-based isomeric dyes by swapping the position of the triphenylamine and acceptor units. It was found that the *N*-butyl group on the benzimidazole unit distorts the chromophore on that side and dictates the optical and electrochemical properties accordingly. The distortion in the donor−acceptor conjugation axis generally reduces the charge transfer interaction between them. In a T-shaped molecular configuration, the arrangement of triphenylamine units on one axis and the acceptor segment on the perpendicular axis reduced the donor−acceptor interaction and conjugation significantly in **7c**. Thus, the absorption peak of the dyes assumed the order **7b** > **7c** > **7a** in line with these estimates. The dyes exhibited a weak solvatochromism confirming the ICT character. Also, the oxidation of **7b** was more difficult in the series due to the stronger donor−acceptor interaction which led to the depletion of electron density form the donor moiety. The structural perturbations and their impact on the optical and electrochemical properties were further quantified by the DFT calculations. The dyes were used as sensitizers in DSSC and found to result promising efficiency in the range 3.45−5.01%

EXPERIMENTAL SECTION

General Methods. The precursor, 3,6-dibromobenzene-1,2-diamine (**1**), required for the synthesis of target compounds was synthesized by a reduction of 4,7-dibromobenzo[*c*][1,2,5]thiadiazole with $NaBH_4$ according to a literature procedure.[47] All other chemicals were procured from commercial sources and used as received. Solvents for photophysical measurements were distilled over suitable dehydrating agents according to standard methods prior to use. All of the compounds were purified by column chromatography using 100−200 mesh silica gel or neutral alumina. ^{1}H and ^{13}C NMR spectra were recorded in NMR spectrometers operating at 400.00 or 500.13 MHz for ^{1}H NMR and 100.00 or 125.77 MHz for ^{13}C NMR. The chemical shifts were calibrated from the residual peaks observed for the deuterated solvents such as chloroform ($CDCl_3$) and dimethyl sulfoxide (DMSO-d_6) at δ 7.26 and 2.52 ppm for ^{1}H and 77.0 and 39.5 ppm for ^{13}C, respectively. High resolution mass spectra were measured using a TOF-Q ESI mass spectrometer in positive ion mode. The optical absorption and emission spectra of the dyes were measured for the freshly prepared air equilibrated solutions at room temperature by using a UV−vis spectrophotometer and spectrofluorimeter, respectively. The IR spectra were recorded by using a FT-IR spectrometer. Cyclic voltammetry (CV) and differential pulse voltammetry (DPV) experiments were performed with an electrochemical analyzer using a conventional three-electrode assembly comprising a glassy carbon working electrode, a platinum wire auxiliary electrode, and a nonaqueous (acetonitrile) $Ag/AgNO_3$ reference electrode. The $E_{1/2}$ values were determined as $(E_p^a + E_p^c)/2$, where E_p^a and E_p^c are the anodic and cathodic peak potentials, respectively. Ferrocene was used as the internal potential marker.

*2-(2,2′-Bithiophen-5-yl)-4,7-dibromo-1H-benzo[d]imidazole (**2**).* A mixture of 3,6-dibromobenzene-1,2-diamine (7.40 g, 27.80 mmol), 2,2′-bithiophene-5-carbaldehyde (4.50 g, 23.16 mmol), and $Na_2S_2O_5$ (13.20 g, 69.60 mmol) in 50 mL of DMF was heated at 95 °C. The reaction was monitored by TLC. After completion of the reaction (24 h), it was poured into ice cold water, and the resulting solid was filtered and dried. It was crystallized from a mixture of dichloromethane/hexane (3:1 v/v) to obtain a light yellow solid; yield 10.00 g, 98%; mp 280 °C; IR (KBr, cm^{-1}) 3076 (υ_{N-H}); ^{1}H NMR (DMSO-d_6, 400.00 MHz) δ 7.11 (dd, J = 5.0, 3.7 Hz, 1 H), 7.31 (s, 2 H), 7.38 (d, J = 3.7 Hz, 1 H), 7.45−7.46 (m, 1 H), 7.57 (dd, J = 5.0, 1.4 Hz, 1 H), 8.06 (d, J = 3.7 Hz, 1 H). ^{13}C NMR (DMSO-d_6, 100.00 MHz) δ 125.0, 125.4, 126.3, 126.7, 128.7, 129.9, 130.7, 135.8, 140.0, 148.2. HRMS (ESI) *m*/*z*: $[M + Na]^+$ Calcd for $C_{15}H_8Br_2N_2S_2Na$ 462.8373; found, 462.8393.

*2-(2,2′-Bithiophen-5-yl)-4,7-dibromo-1-butyl-1H-benzo[d]-imidazole (**3**).* A mixture of 2-(2,2′-bithiophen-5-yl)-4,7-dibromo-1*H*-benzo[*d*]imidazole (9.5 g, 21.6 mmol), *n*-BuBr (5.0 g, 43.2 mmol), potassium carbonate (8.9 g, 64.8 mmol), and 50 mL DMF was heated at 95 °C. After 24 h, it was poured into ice cold water to produce a yellow precipitate. It was purified by column chromatography on silica using dichloromethane/hexane (1:1, v/v) as eluent. Light yellow solid; yield 7.5 g, 75%; mp 162 °C; ^{1}H NMR ($CDCl_3$, 500.13 MHz) δ 0.98 (t, J = 7.5 Hz, 3 H), 1.40−1.47 (m, 2 H), 1.88−1.94 (m, 2 H), 4.69 (t, J = 8.5 Hz, 2 H), 7.06−7.08 (m, 1 H), 7.24 (d, J = 4.0 Hz, 1 H), 7.28−7.33 (m, 4 H), 7.48 (d, J = 3.5 Hz, 1 H). ^{13}C NMR ($CDCl_3$, 100.00 MHz) δ 13.8, 19.7, 34.1, 45.7, 102.1, 113.0, 124.2, 125.0, 125.7, 126.6, 128.2, 128.7, 129.4, 130.0, 133.0, 136.3, 141.5, 143.6, 149.5. HRMS (ESI) *m*/*z*: $[M + Na]^+$Calcd for $C_{19}H_{16}Br_2N_2S_2Na$ 518.8999; found, 518.9007.

DOI: 10.1021/acs.joc.5b02590
J. Org. Chem. 2016, 81, 640−653

*5′-(4,7-Dibromo-1-butyl-1H-benzo[d]imidazol-2-yl)-2,2′-bithiophene-5-carbaldehyde (**4**).* 2-(2,2′-Bithiophen-5-yl)-4,7-dibromo-1-butyl-1*H*-benzo[*d*]imidazole (4.0 g, 8.1 mmol) and DMF (25 mL) were taken in a 100 mL round-bottomed flask, and to this, $POCl_3$ (8.1 mL, 81.0 mmol) was added dropwise via syringe under nitrogen atmosphere at 0 °C. Afterward, the reaction mixture was heated to 65 °C for 8 h. Reaction status was monitored by TLC. After the completion of the reaction, the reaction mixture was poured into ice-cold saturated sodium acetate solution to obtain a yellow precipitate. It was filtered, dried, and crystallized from a mixture of dichloromethane/hexane (1:1, v/v). Yellow solid; yield 6.0 g, 82%; mp 160 °C; IR (KBr, cm^{-1}) 1657 ($\upsilon_{C=O}$); ^{1}H NMR ($CDCl_3$, 500.13 MHz) δ 0.98 (t, J = 7.5 Hz, 3 H), 1.40−1.49 (m, 2 H), 1.89−1.95 (m, 2 H), 4.70 (t, J = 8.0 Hz, 2 H), 7.31−7.34 (m, 2 H), 7.36−7.37 (m, 1 H), 7.42 (d, J = 3.5 Hz, 1 H), 7.54 (d, J = 4.0 Hz, 1 H), 7.72 (d, J = 3.5 Hz, 1 H), 9.90 (s, 1 H); ^{13}C NMR ($CDCl_3$, 125.77 MHz) δ 13.7, 19.6, 33.9, 45.6, 102.1, 113.0, 125.2, 126.4, 126.6, 128.8, 129.4, 132.3, 132.9, 137.2, 139.2, 142.5, 143.4, 145.4, 148.4, 182.4. HRMS (ESI) m/z: $[M + Na]^+$ Calcd for $C_{20}H_{16}Br_2N_2OS_2Na$ 546.8948; found, 546.8964.

*5′-(1-Butyl-4,7-bis(4-(diphenylamino)phenyl)-1H-benzo[d]-imidazol-2-yl)-2,2′-bithiophene-5-carbaldehyde (**5**) and 5′-(4-Bromo-1-butyl-7-(4-(diphenylamino)phenyl)-1H-benzo[d]imidazol-2-yl)-2,2′-bithiophene-5-carbaldehyde (**6**).* In a 100 mL two-necked round-bottomed flask, 4-(diphenylamino)phenylboronic acid (0.61 g, 2.09 mmol), 5′-(4,7-dibromo-1-butyl-1*H*-benzo[*d*]imidazol-2-yl)-2,2′-bithiophene-5-carbaldehyde, **4** (1.0 g, 1.9 mmol), potassium carbonate (0.79 g, 5.7 mmol), and 30 mL of THF/H_2O (3:1, v/v) were taken and purged with nitrogen. After the addition of $Pd(PPh_3)_4$ (90 mg, 2 mol %), the reaction mixture was refluxed for 24 h. On completion of the reaction, it was diluted with dichloromethane and water. The organic layer was separated, dried over anhydrous Na_2SO_4, and the volatiles removed under reduced pressure. The crude solid containing products **5** and **6** were purified by column chromatography on silica using dichloromethane/hexane as eluent. Compound **5**: orange solid; yield 0.21 g, 13%; mp 140 °C; IR (KBr, cm^{-1}) 1659 ($\upsilon_{C=O}$); ^{1}H NMR ($CDCl_3$, 500.13 MHz) δ 0.76 (t, J = 7.5 Hz, 3 H), 0.95−1.01 (m, 2 H), 1.39−1.45 (m, 2 H), 4.20 (t, J = 8.5 Hz, 2 H), 7.02−7.08 (m, 4 H), 7.16−7.23 (m, 13 H), 7.26−7.32 (m, H), 7.34−7.39 (m, 4 H), 7.43 (d, J = 3.5 Hz, 1 H), 7.47 (d, J = 7.5 Hz, 1 H), 7.70 (d, J = 4.0 Hz, 1 H), 8.05 (d, J = 9.0 Hz, 2 H), 9.89 (s, 1 H). ^{13}C NMR ($CDCl_3$, 125.77 MHz) δ 13.5, 19.7, 32.4, 45.5, 121.1, 122.7, 122.8, 123.1, 123.5, 124.4, 124.5, 124.9, 125.3, 126.4, 126.4, 128.3, 129.1, 129.3, 130.0, 130.5, 130.8, 132.1, 132.5, 133.6, 134.4, 137.3, 138.3, 141.3, 142.2, 146.0, 147.0, 147.2, 147.4, 147.5, 147.7, 182.4. HRMS (ESI) m/z: $[M]^+$ Calcd for $C_{56}H_{44}N_4OS_2$ 852.2957; found, 852.2943.

Compound **6**: yellow solid; yield 0.6 g, 46.1%; mp 238 °C; IR (KBr, cm^{-1}) 1653 ($\upsilon_{C=O}$); ^{1}H NMR ($CDCl_3$, 400.00 MHz) δ 0.73 (t, J = 7.6 Hz, 3 H), 0.92−0.99 (m, 2 H), 1.32−1.39 (m, 2 H), 4.13 (t, J = 7.6 Hz, 2 H), 7.00 (d, J = 8.0 Hz, 1 H), 7.04−7.08 (m, 1 H), 7.12−7.15 (m, 7 H), 7.25−7.30 (m, 6 H), 7.34 (d, J = 4.0 Hz, 1 H), 7.38 (d, J = 4.0 Hz, 1 H), 7.45 (d, J = 3.6 Hz, 1 H), 7.49 (d, J = 7.6 Hz, 1 H), 7.70 (d, J = 3.6 Hz, 1 H), 9.88 (s, 1 H). ^{13}C NMR ($CDCl_3$, 100.00 MHz) δ 13.7, 19.8, 32.6, 46.0, 112.5, 122.8, 123.5, 124.7, 125.3, 125.5, 126.5, 127.0, 129.4, 129.5, 130.5, 137.5, 139.0, 142.4, 142.5, 145.9, 147.6, 147.9, 148.1, 182.7 HRMS (ESI) m/z: $[M + Na]^+$ Calcd for $C_{38}H_{30}BrN_3OS_2Na$ 710.0911; found, 710.0904.

*4-(4,7-Dibromo-1H-benzo[d]imidazol-2-yl)-N,N-diphenylaniline (**8**).* It was synthesized by following the procedure described above for compound **2**, except using 4-(diphenylamino)benzaldehyde instead of 2-(2,2′-bithiophen-5-yl)-4,7-dibromo-1*H*-benzo[*d*]imidazole. Off white solid; yield 90%; mp 325 °C; IR (KBr, cm^{-1}) 3053 (υ_{N-H}); ^{1}H NMR (DMSO-*d*6, 500.13 MHz) δ 7.05 (d, J = 8.5 Hz, 2 H), 7.12−7.17 (m, 6 H), 7.33−7.40 (m, 6 H), 8.19 (d, J = 8.5 Hz, 2 H), 13.07 (s, 1 H). ^{13}C NMR (DMSO-d_6, 125.77 MHz) δ 121.5, 122.4, 124.7, 125.6, 129.3, 130.3, 147.0, 149.9, 153.6. HRMS (ESI) m/z: $[M]^+$ Calcd for $C_{25}H_{17}Br_2N_3$ 518.9769; found, 518.9780.

*4-(4,7-Dibromo-1-butyl-1H-benzo[d]imidazol-2-yl)-N,N-diphenylaniline (**9**).* It was prepared by following the procedure described above for **3**, but 4-(4,7-dibromo-1*H*-benzo[*d*]imidazol-2-yl)-*N*,*N*-diphenylaniline was used instead of 2-(2,2′-bithiophen-5-yl)-4,7-dibromo-1*H*-benzo[*d*]imidazole. An off white solid appeared; yield 85%; mp 140 °C; ^{1}H NMR (DMSO-*d*6, 500.13 MHz) δ 0.73 (t, J = 7.0 Hz, 3 H), 1.08−1.15 (m, 2H), 1.63−1.69 (m, 2 H), 4.51 (t, J = 7.5 Hz, 3 H), 7.06 (d, J = 9.0 Hz, 2 H), 7.13−7.16 (m, 6 H), 7.37−7.40 (m, 6 H), 7.63 (d, J = 8.5 Hz, 2 H). ^{13}C NMR ($CDCl_3$, 125.77 MHz) δ 13.6, 19.4, 34.1, 45.5, 102.4, 113.0, 122.1, 122.7, 123.9, 125.2, 126.2, 128.1, 129.6, 130.8, 132.8, 143.9, 147.1, 149.7, 156.4. HRMS (ESI) m/z: $[M]^+$ Calcd for $C_{29}H_{25}Br_2N_3$ 575.0395; found, 575.0425.

*4,4′-(4-Bromo-1-butyl-1H-benzo[d]imidazole-2,7-diyl)bis(N,N-diphenylaniline) (**10**).* It was synthesized by following the procedure described above for **6**, except using of 4-(4,7-dibromo-1-butyl-1*H*-benzo[*d*]imidazol-2-yl)-*N*,*N*-diphenylaniline instead of 5′-(4,7-dibromo-1-butyl-1*H*-benzo[*d*]imidazol-2-yl)-2,2′-bithiophene-5-carbaldehyde. Off white solid; yield 50%; mp 180 °C; ^{1}H NMR ($CDCl_3$, 500.13 MHz) δ 0.64 (t, J = 7.0 Hz, 3 H), 0.77−0.85 (m, 2 H), 1.16−1.24 (m, 2 H), 4.11 (t, J = 7.5 Hz, 2 H), 7.01 (d, J = 8.0 Hz, 1 H), 7.05−7.10 (m, 4 H), 7.14−7.17 (m, 12 H), 0.7.33 (m, 10 H), 7.49 (d, J = 8.0 Hz, 1 H), 7.55 (d, J = 8.5 Hz, 2 H). ^{13}C NMR ($CDCl_3$, 125.77 MHz) δ 13.6, 19.6, 32.5, 45.7, 121.1, 122.4, 122.7, 123.1, 123.6, 123.7, 124.5, 124.5, 125.1, 125.3, 125.6, 125.6, 129.2, 129.4, 129.5, 130.2, 130.7, 130.8, 130.9, 132.9, 133.3, 146.8, 147.3, 147.7, 147.9, 149.1, 155.3. HRMS (ESI) m/z: $[M + Na]^+$ Calcd for $C_{47}H_{39}BrN_4Na$ 761.2256; found, 761.2273.

*5′-(1-Butyl-2,7-bis(4-(diphenylamino)phenyl)-1H-benzo[d]-imidazol-4-yl)-2,2′-bithiophene-5-carbaldehyde (**11**).* In a 100 mL round-bottomed flask, 4,4′-(4-bromo-1-butyl-1*H*-benzo[*d*]imidazole-2,7-diyl)bis(*N*,*N*-diphenylaniline) **10**, (0.40 g, 0.54 mmol), (5′-(1,3-dioxolan-2-yl)-2,2′-bithiophen-5-yl)tributylstannane (0.38 g, 0.7 mmol), and 6 mL of DMF were taken and purged with nitrogen. After the addition of $Pd(PPh_3)_2Cl_2$ (7 mg, 1 mol %), the reaction mixture was heated at 90 °C for 18 h. After the completion of the reaction, it was poured into ice cold water and extracted with dichloromethane. The solvent was removed, and the resulting residue suspended in 5 mL of glacial acetic acid and stirred for 1 h at 60 °C. Then, 5 mL of water was added to the mixture and further heated for 1 h at the same temperature. Finally, it was extracted with dichloromethane and the volatiles removed to obtain a residue. It was purified by column chromatography on neutral alumina using dichloromethane/hexane (1:1, v/v) as eluent. Orange solid; yield 35%; mp 180 °C; IR (KBr, cm^{-1}) 1662 ($\upsilon_{C=O}$); ^{1}H NMR ($CDCl_3$, 400.00 MHz) δ 0.65 (t, J = 7.3 Hz, 3 H), 0.80−0.86 (m, 2 H), 1.20−1.28 (m, 2 H), 4.11 (t, J = 7.8 Hz, 2 H), 7.03−7.14 (m, 3 H), 7.13−7.23 (m, 13 H), 7.25−7.39 (m, 12 H), 7.41 (d, J = 3.4 Hz, 1 H), 7.59−7.69 (m, 4 H), 8.06 (d, J = 3.6 Hz, 1 H), 9.84 (s, 1 H). ^{13}C NMR ($CDCl_3$, 400.00 MHz) δ 13.4, 19.4, 32.3, 45.8, 119.3, 122.0, 122.8, 123.1, 123.3, 123.7, 123.8, 124.40, 125.1, 126.6, 126.8, 127.0, 129.3, 129.4, 130.6, 132.5, 133.2, 135.4, 137.6, 140.8, 140.9, 149.9, 147.0, 147.4, 147.5, 148.0, 149.2, 156.6, 182.4. HRMS (ESI) m/z: $[M + H]^+$ Calcd for $C_{56}H_{44}N_4OS_2$ 853.2990; found, 853.2998.

*5′-(4-Bromo-1-butyl-2-(4-(diphenylamino)phenyl)-1H-benzo[d]-imidazol-7-yl)-2,2′-bithiophene-5-carbaldehyde (**12**).* It was synthesized by following the procedure described above for **11**, except using of 4-(4,7-dibromo-1-butyl-1*H*-benzo[*d*]imidazol-2-yl)-*N*,*N*-diphenylaniline instead of 4,4′-(4-bromo-1-butyl-1*H*-benzo[*d*]imidazole-2,7-diyl)-bis(*N*,*N*-diphenylaniline). Yellow solid; yield 0.17 g, 20%; mp 275 °C; IR (KBr, cm^{-1}) 1656 ($\upsilon_{C=O}$); ^{1}H NMR ($CDCl_3$, 400.00 MHz) δ 0.57 (t, J = 7.3 Hz, 3 H), 0.77−0.82 (m, 2 H), 1.24−1.28 (m, 2 H), 4.11 (t, J = 7.6 Hz, 2 H), 7.06−7.14 (m, 10 H), 7.25−7.31 (m, 5 H), 7.37 (d, J = 3.6 Hz, 1 H), 7.49 (d, J = 7.8 Hz, 1 H), 7.53 (d, J = 8.7 Hz, 2 H), 7.70 (d, J = 4.1 Hz, 1 H), δ 9.88 (s, 1 H). ^{13}C NMR ($CDCl_3$, 100.00 MHz) δ 13.3, 19.4, 32.7, 46.1, 114.38, 117.3, 122.1, 122.7, 123.8, 124.4, 125.0, 125.1, 125.7, 127.1, 129.4, 130.7, 133.3, 136.7, 137.4, 140.6, 141.9, 142.8, 146.4, 147.0, 149.5, 156.6, 182.6. HRMS (ESI) m/z: $[M + Na]^+$ Calcd for $C_{38}H_{30}BrN_3OS_2Na$ 710.0911; found, 710.0901.

*5′-(1-Butyl-2,4-bis(4-(diphenylamino)phenyl)-1H-benzo[d]-imidazol-7-yl)-2,2′-bithiophene-5-carbaldehyde (**13**).* It was synthesized by following the procedure described above for **6**, except using 5′-(4-bromo-1-butyl-2-(4-(diphenylamino)phenyl)-1*H*-benzo[*d*]-imidazol-7-yl)-2,2′-bithiophene-5-carbaldehyde instead of 5′-(4,7-dibromo-1-butyl-1*H*-benzo[*d*]imidazol-2-yl)-2,2′-bithiophene-5-carbaldehyde. Yellow solid; yield 51%; mp 145 °C; IR (KBr, cm^{-1}) 1651 ($\upsilon_{C=O}$); ^{1}H NMR ($CDCl_3$, 400.00 MHz) δ 0.59 (t, J = 4.8 Hz, 3H), 0.79−0.84 (m, 2 H), 1.27−1.32 (m, 2 H), 4.17 (d, J = 8.0 Hz, 2 H),

DOI: 10.1021/acs.joc.5b02590
J. Org. Chem. 2016, 81, 640−653

6.98−7.10 (m, 4 H), 7.11−7.18 (m, 13 H), 7.22−7.32 (m, 10 H), 7.39 (d, J = 3.6 Hz, 1 H), 7.43 (d, J = 7.6 Hz, 1 H), 7.56 (d, J = 7.2 Hz, 2 H), 7.70 (d, J = 4.4 Hz, 1 H), 8.01 (dd, J = 8.8 Hz, 2.0 Hz, 2 H), 9.88 (s, 1 H). ^{13}C NMR ($CDCl_3$, 100.00 MHz) δ 13.3, 19.4, 32.7, 45.9, 116.3, 120.9, 122.1, 122.8, 123.4, 123.6, 123.6, 124.2, 124.6, 125.1, 125.7, 129.2, 129.4, 130.2, 130.6, 132.0, 132.6, 133.8, 136.2, 137.4, 141.7, 141.9, 142.0, 146.8, 147.1, 147.7, 149.2, 155.8.182.5. HRMS (ESI) m/z: $[M + H]^+$ Calcd for $C_{56}H_{44}N_4OS_2$ 853.2990; found, 853.3008.

*(Z)-3-(5′-(1-Butyl-4,7-bis(4-(diphenylamino)phenyl)-1H-benzo[d]-imidazol-2-yl)-2,2′-bithiophen-5-yl)-2-cyanoacrylic Acid (**7a**).* A mixture of 5′-(1-butyl-4,7-bis(4-(diphenylamino)phenyl)-1*H*-benzo-[*d*]imidazol-2-yl)-2,2′-bithiophene-5-carbaldehyde (0.20 g, 0.23 mmol) cyanoacetic acid (0.03 g, 0.35 mmol), ammonium acetate (100 mg), and acetic acid (5 mL) was heated at 80 °C for 24 h. After the completion of the reaction, it was poured into water, filtered, and dried. Red solid; yield 0.15 g, 85%; mp 276 °C; IR (KBr, cm^{-1}) 2219 ($\upsilon_{C\equiv N}$), 3438 (υ_{O-H}), 1679 ($\upsilon_{C=O}$); ^{1}H NMR (DMSO-d_6, 500.13 MHz) δ 0.66 (t, J = 7.5 Hz, 3 H), 0.87−0.92 (m, 2 H), 1.29−1.32 (m, 2 H), 4.19 (t, J = 8.5 Hz, 2 H), 7.08−7.11 (m, 16 H), 7.15 (d, J = 7.5 Hz, 1 H), 7.33−7.36 (m, 8 H), 7.44−7.48 (m, 3 H), 7.68−7.71 (m, 3 H), 8.00 (d, J = 4.0 Hz, 1 H), 8.06 (d, J = 8.5 Hz, 2 H), 8.51 (s, 1 H). ^{13}C NMR (DMSO-d_6, 125.77 MHz) δ 13.7, 19.5, 32.1, 45.6, 117.0, 121.2, 123.0, 123.1, 123.7, 123.8, 124.6, 124.7, 125.8, 126.6, 128.2, 129.8, 130.3, 131.1, 132.2, 132.6, 133.8, 134.1, 135.3, 137.8, 141.2, 141.5, 144.7, 146.6, 147.0, 147.3, 147.4, 147.5, 147.6, 163.9. HRMS (ESI) m/z: $[M + Na]^+$ Calcd for $C_{59}H_{45}N_5O_2S_2Na$ 942.2912; found, 942.2939.

*(E)-3-(5′-(1-Butyl-2,7-bis(4-(diphenylamino)phenyl)-1H-benzo[d]-imidazol-4-yl)-2,2′-bithiophen-5-yl)-2-cyanoacrylic Acid (**7b**).* It was synthesized by following the procedure described above for **7a**, except using 5′-(1-butyl-2,7-bis(4-(diphenylamino)phenyl)-1*H*-benzo[*d*]-imidazol-4-yl)-2,2′-bithiophene-5-carbaldehyde instead of 5′-(1-butyl-4,7-bis(4-(diphenylamino)phenyl)-1*H*-benzo[*d*]imidazol-2-yl)-2,2′-bithiophene-5-carbaldehyde. Orange solid; yield 90%; mp 283 °C; IR (KBr, cm^{-1}) 2216 ($\upsilon_{C\equiv N}$), 3436 (υ_{O-H}), 1701 ($\upsilon_{C=O}$); ^{1}H NMR (DMSO-d_6, 500.13 MHz) δ 0.54 (t, J = 7.0 Hz, 3 H), 0.68−0.74 (m, 2 H), 1.07−1.13 (m, 2 H), 4.04 (t, J = 7.5 Hz, 2 H), 7.07−7.10 (m, 10 H), 7.14−7.16 (m, 7 H), 7.32−7.40 (m, 8 H), 7.47 (d, J = 8.5 Hz, 2 H), 7.62 (d, J = 4.0 Hz, 1 H), 7.66−7.69 (m, 3 H), 7.76 (d, J = 8.0 Hz, 1 H), 7.98 (d, J = 4.0 Hz, 1 H), 8.15 (d, J = 4.0 Hz, 1 H), 8.48 (s, 1 H). ^{13}C NMR (DMSO-d_6, 125.77 MHz) δ 13.0, 18., 31.6, 45.25, 116.7, 121.1, 122.4, 122.6, 122.9, 123.3, 124.0, 125.0, 126.5, 127.2, 127.4, 129.6, 132.1, 132.7, 133.7, 134.9, 140.1, 142.2, 146.3, 146.5, 146.9, 147.0, 148.7, 155.1, 163.7. HRMS (ESI) m/z: $[M + Na]^+$ Calcd for $C_{59}H_{45}N_5O_2S_2Na$ 942.2912; found, 942.2911.

*3-(5′-(1-Butyl-2,4-bis(4-(diphenylamino)phenyl)-1H-benzo[d]-imidazol-7-yl)-2,2′-bithiophen-5-yl)-2-cyanoacrylic Acid (**7c**).* The title compound was synthesized by following the procedure described above for **7a**, except using of 5′-(1-butyl-2,4-bis(4-(diphenylamino)-phenyl)-1*H*-benzo[*d*]imidazol-7-yl)-2,2′-bithiophene-5-carbaldehyde instead of 5′-(1-butyl-4,7-bis(4-(diphenylamino)phenyl)-1*H*-benzo[*d*]-imidazol-2-yl)-2,2′-bithiophene-5-carbaldehyde. Yellow solid; yield 80%; mp 271 °C; IR (KBr, cm^{-1}) 2215 ($\upsilon_{C\equiv N}$), 3437 (υ_{O-H}), 1700 ($\upsilon_{C=O}$); ^{1}H NMR (DMSO-d_6, 500.13 MHz) δ 0.48 (t, J = 7.0 Hz, 3 H), 0.66−0.73 (m, 2 H), 1.15−1.21 (m, 2 H), 4.16 (t, J = 9.0 Hz, 2 H), 7.02−7.13 (m, 16 H), 7.30−7.38 (m, 10 H), 7.47 (d, J = 8.0 Hz, 1 H), 7.60−7.63 (m, 3 H), 7.68 (d, J = 3.5 Hz, 1 H), 8.00 (d, J = 4.0 Hz, 1 H), 8.05 (d, J = 8.5 Hz, 2 H), 8.50 (s, 1 H). ^{13}C NMR (DMSO-d_6, 125.77 MHz) δ 13.4, 19.2, 32.2, 45.8, 116.9, 116.99, 120.8, 121.6, 123.1, 123.6, 123.7, 124.5, 124.6, 125.4, 125.6, 125.7, 126.8, 127.3, 130.0, 130.2, 130.6, 130.7, 131.2, 131.6, 132.1, 133.66, 134.62, 135.86, 141.41, 141.74, 141.84, 145.61, 146.74, 146.99, 147.08, 147.50, 149.1, 155.8, 164.0. HRMS (ESI) m/z: $[M + Na]^+$ Calcd for $C_{59}H_{45}N_5O_2S_2Na$ 942.2912; found, 942.2937.

Fabrication and Characterization of DSSCs. A fluorine-doped SnO_2 conducting glass electrode (FTO, 7 Ω sq^{-1}, transmittance ca. 80%) was first cleaned with a neutral cleaner and then washed with deionized water, acetone, and isopropyl alcohol, sequentially. The conducting surface of the FTO was treated with a solution of titanium tetraisopropoxide (1 g) in 2-methoxyethanol (3 g) to obtain a good mechanical contact between the conducting glass and TiO_2 film, as well as to isolate the conducting glass surface from the electrolyte. TiO_2 pastes were coated onto the treated conducting glass by using the doctor blade technique. To coat each TiO_2 layer, the dried TiO_2 film was gradually heated to 450 °C under an oxygen atmosphere and subsequently sintered at that temperature for 30 min. The TiO_2 photoanodes of the DSSCs employed in the experiments were composed of a 12 μm thickness and 20 nm particle size TiO_2 layer/4 μm scattering TiO_2 layer. After sintering at 450 °C and cooling to 80 °C, the TiO_2 film was immersed in a 3 × 10^{-4} M solution of dye at room temperature for 24 h. The standard ruthenium complex, **N719**, was dissolved in acetonitrile and *tert*-butyl alcohol (1:1) to make a reference dye solution. Various organic dye solutions were prepared in a mixing solvent containing MeCN/*tert*-BuOH/DMSO (3.5:3.5:3 v/v). Then, the prepared TiO_2/dye electrode was placed on a platinum-sputtered conducting glass electrode (ITO, 7 Ω sq^{-1}), thus keeping the two electrodes separated by a 25 μm thick Surlyn. The two electrodes were then sealed by heating. A mixture of 0.1 M GuSCN, 1.2 M 1-propyl-2,3-dimethylimidazolium iodide (DMPII), 0.035 M I_2, and 0.5 M *tert*-butylpyridine (TBP) in ACN/3-methoxypropionitrile (MPN) (8:2) was used as the electrolyte. The electrolyte was injected into the gap between the electrodes by capillarity; the electrolyte-injecting hole was previously made in the counter electrode with a drilling machine, and the hole was sealed with hot-melt glue after the injection of the electrolyte. The surface of the DSSC was covered by a mask with a light-illuminated area of 0.16 cm^2 and then illuminated by a class A quality solar simulator. Incident light intensity (100 mW cm^{-2}) was calibrated with a standard silicon cell. Photocurrent−voltage curves of the DSSCs were obtained with a potentiostat/galvanostat. The thickness of the TiO_2 film was judged by scanning electron microscopic images (SEM). For UV absorption spectra, dye molecules were coated on the TiO_2 films, and the corresponding spectra were obtained by using an UV/vis spectrophotometer equipped with an integrating sphere. Electrochemical impedance spectra (EIS) were obtained from the potentiostat/galvanostat, equipped with a FRA2 module, under a constant light illumination of 100 mW cm^{-2}. The frequency range explored was 10 MHz to 65 kHz. The applied bias voltage was set at the open-circuit voltage of the DSSC between the ITO-Pt counter electrode and the FTO-TiO_2 dye working electrode, starting from the short-circuit condition; the corresponding alternating current (AC) amplitude was 10 mV. The impedance spectra were analyzed by using an equivalent circuit model. IPCE curves were obtained under short-circuit conditions. The light source was a class A quality solar simulator (PEC-L11, AM 1.5 G); light was focused through a monochromator onto the photovoltaic cell. The monochromator was incremented through the visible spectrum to generate the IPCE (λ) as defined by IPCE (λ) = 1240 (J_{SC}/ϕ), where λ is the wavelength, J_{SC} is the short-circuit photocurrent density (mAcm^{-2}) recorded with a potentiostat/galvanostat, and ϕ is the incident radiative flux (Wm^{2-}) measured with an optical detector and a power meter.

■ ASSOCIATED CONTENT

Supporting Information

The Supporting Information is available free of charge on the ACS Publications website at DOI: 10.1021/acs.joc.5b02590.

Absorption and emission spectra of the compounds recorded in different solvents; ^{1}H and ^{13}C NMR spectra of the synthesized compounds; and Cartesian coordinates of the optimized structures (PDF)

Crystallographic information file for compound **6** (CIF)

■ AUTHOR INFORMATION

Corresponding Author

*E-mail: krjt8fcy@iitr.ac.in.

Notes

The authors declare no competing financial interest.

DOI: 10.1021/acs.joc.5b02590
J. Org. Chem. 2016, 81, 640−653

■ ACKNOWLEDGMENTS

K.R.J.T. is thankful to DST, New Delhi (DST/TSG/PT/2013/09) for financial support. G.B.B. acknowledges the Senior Research Fellowship (SRF) from CSIR, New Delhi. We are thankful to DST for the purchase of an ESI mass spectrometer via the FIST grant to the Chemistry Department, IIT Roorkee.

■ REFERENCES

(1) O'Regan, B.; Grätzel, M. *Nature* **1991**, *353*, 737.
(2) (a) Hagfeldt, A.; Boschloo, G.; Sun, L.; Kloo, L.; Pettersson, H. *Chem. Rev.* **2010**, *110*, 6595. (b) Stengel, I.; Pootrakulchote, N.; Dykeman, R. R.; Mishra, A.; Zakeeruddin, S. M.; Dyson, P. J.; Grätzel, P. J.; Bäuerle, P. *Adv. Energy Mater.* **2012**, *2*, 1004. (c) Chen, C.-Y.; Pootrakulchote, N.; Hung, T.-H.; Tan, C.-J.; Tsai, H.-H.; Zakeeruddin, S. M.; Wu, C.-G.; Grätzel, M. *J. Phys. Chem. C* **2011**, *115*, 20043. (d) Feldt, S. M.; Gibson, E. A.; Gabrielsson, E.; Sun, L.; Boschloo, G.; Hagfeldt, A. *J. Am. Chem. Soc.* **2010**, *132*, 16714. (e) Reynal, A.; Palomares, E. *Eur. J. Inorg. Chem.* **2011**, *2011*, 4509. (f) Chen, J.-G.; Wu, S.-J.; Li, J.-Y.; Wu, C.-G.; Ho, K.-C. *Angew. Chem., Int. Ed.* **2008**, *47*, 7342.
(3) (a) Urbani, M.; Grätzel, M.; Nazeeruddin, M. K.; Torres, T. *Chem. Rev.* **2014**, *114*, 12330. (b) Li, L.-L.; Diau, E. W.-G. *Chem. Soc. Rev.* **2013**, *42*, 291. (c) Higashino, T.; Imahori, H. *Dalton Trans.* **2015**, *44*, 448.
(4) (a) Martin-Gomis, L.; Fernández-Lázaro, F.; Sastre-Santos, A. *J. Mater. Chem. A* **2014**, *2*, 15672. (b) Singh, V. K.; Kanaparthi, R. K.; Giribabu, L. *RSC Adv.* **2014**, *4*, 6970.
(5) (a) Luo, S.; Daoud, W. A. *J. Mater. Chem. A* **2015**, *3*, 8992. (b) Wang, B.; Xiao, X.; Chen, T. *Nanoscale* **2014**, *6*, 12287. (c) Gao, P.; Grätzel, M.; Nazeeruddin, M. K. *Energy Environ. Sci.* **2014**, *7*, 2448.
(6) (a) Clifford, J. N.; MartInez-Ferrero, E.; Viterisi, A.; Palomares, E. *Chem. Soc. Rev.* **2011**, *40*, 1635. (b) Yen, Y.-S.; Chou, H. H.; Chen, Y.-C.; Hsu, C.-Y.; Lin, J. T. *J. Mater. Chem.* **2012**, *22*, 8734.
(7) (a) Jeon, N. J.; Lee, H. G.; Kim, Y. C.; Seo, J.; Noh, J. H.; Lee, J.; Seok, S. I. *J. Am. Chem. Soc.* **2014**, *136*, 7837. (b) Burschka, J.; Pellet, N.; Moon, S.-J.; Humphry-Baker, R.; Gao, P.; Nazeeruddin, M. K.; Grätzel, M. *Nature* **2013**, *499*, 316. (c) Eperon, G. E.; Stranks, S. D.; Menelaou, C.; Johnston, M. B.; Herz, L. M.; Snaith, H. J. *Energy Environ. Sci.* **2014**, *7*, 982. (d) Docampo, P.; Ball, J. M.; Darwich, M.; Eperon, G. E.; Snaith, H. J. *Nat. Commun.* **2013**, *4*, 2761. (e) Liu, D.; Kelly, T. L. *Nat. Photonics* **2013**, *8*, 133. (f) Green, M. A.; Ho-Baillie, A.; Snaith, H. J. *Nat. Photonics* **2014**, *8*, 506. (g) Zhou, H.; Chen, Q.; Li, G.; Luo, S.; Song, T.-b.; Duan, H.-S.; Hong, Z.; You, J.; Liu, Y.; Yang, Y. *Science* **2014**, *345*, 542. (h) Im, J.-H.; Jang, I.-H.; Pellet, N.; Grätzel, M.; Park, N.-G. *Nat. Nanotechnol.* **2014**, *2*, 705. (i) Nie, W.; Tsai, H.; Asadpour, R.; Blancon, J.-C.; Neukirch, A. J.; Gupta, G.; Crochet, J. J.; Chhowalla, M.; Tretiak, S.; Alam, M. A.; Wang, H.-L.; Mohite, A. D. *Science* **2015**, *347*, 522.
(8) (a) Ooyama, Y.; Harima, Y. *Eur. J. Org. Chem.* **2009**, *2009*, 2903. (b) Mishra, A.; Fischer, M. K. R.; Bäuerle, P. *Angew. Chem., Int. Ed.* **2009**, *48*, 2474. (c) Ning, Z.; Fu, Y.; Tian, H. *Energy Environ. Sci.* **2010**, *3*, 1170. (d) Hamann, T. W.; Jensen, R. A.; Martinson, F.; Ryswyka, H. V.; Hupp, J. T. *Energy Environ. Sci.* **2008**, *1*, 66.
(9) (a) Kakiage, K.; Aoyama, Y.; Yano, T.; Oya, K.; Kyomen, T.; Hanaya, M. *Chem. Commun.* **2015**, *51*, 6315. (b) Zhang, M.; Wang, Y.; Xu, M.; Ma, W.; Li, R.; Wang, P. *Energy Environ. Sci.* **2013**, *6*, 2944. (c) Kakiage, K.; Aoyama, Y.; Yano, T.; Otsuka, T.; Kyomen, T.; Unno, M.; Hanaya, M. *Chem. Commun.* **2014**, *50*, 6379. (d) Zhang, G.; Bala, H.; Cheng, Y.; Shi, D.; Lv, X.; Yu, Q.; Wang, P. *Chem. Commun.* **2009**, 2198. (e) Tan, L.-L.; Huang, J.-F.; Shen, Y.; Xiao, L.-M.; Liu, J.-M.; Kuang, D.-B.; Su, C.-Y. *J. Mater. Chem. A* **2014**, *2*, 8988. (f) Zeng, W.; Cao, Y.; Bai, Y.; Wang, Y.; Shi, Y.; Zhang, M.; Wang, F.; Pan, C.; Wang, P. *Chem. Mater.* **2010**, *22*, 1915. (g) Qin, C.; Wong, W.-Y.; Han, L. *Chem. - Asian J.* **2013**, *8*, 1706.
(10) (a) Wu, Y.; Zhu, W. *Chem. Soc. Rev.* **2013**, *42*, 2039. (b) Liang, M.; Chen, J. *Chem. Soc. Rev.* **2013**, *42*, 3453. (c) Lee, C.-P.; Lin, R. Y.-Y.; Lin, L.-Y.; Li, C.-T.; Chu, T.-C.; Sun, S.-S.; Lin, J. T.; Ho, K.-C. *RSC Adv.* **2015**, *5*, 23810. (d) Ooyama, Y.; Harima, Y. *ChemPhysChem* **2012**, *13*, 4032.
(11) (a) Manfredi, N.; Cecconi, B.; Abbotto, A. *Eur.—J. Org. Chem.* **2014**, *2014*, 7069. (b) Hung, W.-I.; Liao, Y.-Y.; Lee, T.-H.; Ting, Y.-C.; Ni, J.-S.; Kao, W.-S.; Lin, J. T.; Wei, T.-C.; Yen, Y.-S. *Chem. Commun.* **2015**, *51*, 2152.
(12) (a) Pei, K.; Wu, Y.; Li, H.; Geng, Z.; Tian, H.; Zhu, W.-H. *ACS Appl. Mater. Interfaces* **2015**, *7*, 5296. (b) Zhang, S.; Islam, A.; Yang, X.; Qin, C.; Zhang, K.; Numata, Y.; Chen, H.; Han, L. *J. Mater. Chem. A* **2013**, *1*, 4812. (c) Yella, A.; Lee, H.-W.; Tsao, H. N.; Yi, C.; Chandiran, A. K.; Nazeeruddin, M. K.; Diau, E. W.-G.; Yeh, C.-Y.; Zakeeruddin, S. M.; Grätzel, M. *Science* **2011**, *334*, 629.
(13) (a) Chen, C.; Yang, X.; Cheng, M.; Zhang, F.; Zhao, J.; Sun, L. *ACS Appl. Mater. Interfaces* **2013**, *5*, 10960. (b) Zhang, X.; Mao, J.; Wang, D.; Li, X.; Yang, J.; Shen, Z.; Wu, W.; Li, J.; Ågren, H.; Hua, J. *ACS Appl. Mater. Interfaces* **2015**, *7*, 2760. (c) Roiati, V.; Giannuzzi, R.; Lerario, G.; Marco, L. D.; Agosta, R.; Iacobellis, R.; Grisorio, R.; Suranna, G. P.; Listorti, A.; Gigli, G. *J. Phys. Chem. C* **2015**, *119*, 6956. (d) Xia, Q.; Liang, M.; Tan, Y.; Gao, W.; Ouyang, L.; Ge, G.; Sun, Z.; Xue, S. *Org. Electron.* **2015**, *17*, 285. (e) Yang, J.; Ganesan, P.; Teuscher, J.; Moehl, T.; Kim, Y. J.; Yi, C.; Comte, P.; Pei, K.; Holcombe, T. W.; Nazeeruddin, M. K.; Hua, J.; Zakeeruddin, S. M.; Tian, H.; Grätzel, M. *J. Am. Chem. Soc.* **2014**, *136*, 5722.
(14) (a) Nishida, J.-I.; Masuko, T.; Cui, Y.; Hara, K.; Shibuya, H.; Ihara, M.; Hosoyama, T.; Goto, R.; Mori, S.; Yamashita, Y. *J. Phys. Chem. C* **2010**, *114*, 17920. (b) Lu, X.; Feng, Q.; Lan, T.; Zhou, G.; Wang, Z. S. *Chem. Mater.* **2012**, *24*, 3179. (c) Hua, Y.; He, J.; Zhang, C.; Qin, C.; Han, L.; Zhao, J.; Chen, T.; Wong, W.-Y.; Wong, W.-K.; Zhu, X. *J. Mater. Chem. A* **2015**, *3*, 3103.
(15) (a) Koumura, N.; Wang, Z.-S.; Mori, S.; Miyashita, M.; Suzuki, E.; Hara, K. *J. Am. Chem. Soc.* **2006**, *128*, 14256. (b) Yum, J.-H.; Hagberg, D. P.; Moon, S.-J.; Karlsson, K. M.; Marinado, T.; Sun, L.; Hagfeldt, A.; Nazeeruddin, M. K.; Grätzel, M. *Angew. Chem., Int. Ed.* **2009**, *48*, 1576. (c) Hua, Y.; Chang, S.; Huang, D.; Zhou, X.; Zhu, X.; Zhao, J.; Chen, T.; Wong, W.-Y.; Wong, W.-K. *Chem. Mater.* **2013**, *25*, 2146. (d) Cheng, M.; Yang, X.; Zhang, F.; Zhao, J.; Sun, L. *J. Phys. Chem. C* **2013**, *117*, 9076. (e) Huang, J.-F.; Liu, J.-M.; Tan, L.-L.; Chen, Y.-F.; Shen, Y.; Xiao, L.-M.; Kuang, D.-B.; Su, C.-Yo. *Dyes Pigm.* **2015**, *114*, 18. (f) Wang, Z. S.; Koumura, N.; Cui, Y.; Takahashi, M.; Sekiguchi, H.; Mori, A.; Kubo, T.; Furube, A.; Hara, K. *Chem. Mater.* **2008**, *20*, 3993. (g) Hara, K.; Wang, Z. S.; Cui, Y.; Furube, A.; Koumura, N. *Energy Environ. Sci.* **2009**, *2*, 1109.
(16) (a) Huang, Z.-S.; Feng, H.-L.; Zang, X.-F.; Iqbal, Z.; Zeng, H.; Kuang, D.-B.; Wang, L.; Meier, H.; Cao, D. *J. Mater. Chem. A* **2014**, *2*, 15365. (b) Ni, J.-S.; You, J.-H.; Hung, W.-I.; Kao, W.-S.; Chou, H.-H.; Lin, J. T. *ACS Appl. Mater. Interfaces* **2014**, *6*, 22612.
(17) (a) Cai, N.; Zhang, J.; Xu, M.; Zhang, M.; Wang, P. *Adv. Funct. Mater.* **2013**, *23*, 3539. (b) Bai, Y.; Zhang, J.; Zhou, D.; Wang, Y.; Zhang, M.; Wang, P. *J. Am. Chem. Soc.* **2011**, *133*, 11442.
(18) Tsao, H. N.; Yi, C.; Moehl, T.; Yum, J.-H.; Zakeeruddin, S. M.; Nazeeruddin, M. K.; Grätzel, M. *ChemSusChem* **2011**, *4*, 591.
(19) (a) Wang, Z.-S.; Li, F.-Y.; Huang, C.-H. *J. Phys. Chem. B* **2005**, *109*, 10957. (b) Teng, C.; Yang, X.; Yuan, C.; Li, C.; Chen, R.; Tian, H.; Li, S.; Hagfeldt, A.; Sun, L. *Org. Lett.* **2009**, *11*, 5542. (c) Teng, C.; Yang, X.; Li, S.; Cheng, M.; Hagfeldt, A.; Wu, L.-Z.; Sun, L. *Chem. - Eur. J.* **2010**, *16*, 13127.
(20) (a) Hara, K.; Dan-oh, Y.; Kasada, C.; Ohga, Y.; Shinpo, A.; Suga, S.; Sayama, K.; Arakawa, H. *Langmuir* **2004**, *20*, 4205. (b) Wang, Z.-S.; Cui, Y.; Dan-oh, Y.; Kasada, C.; Shinpo, A.; Hara, K. *J. Phys. Chem. C* **2007**, *111*, 7224. (c) Kusama, H.; Sayama, K. *J. Phys. Chem. C* **2012**, *116*, 23906.
(21) Chaurasia, S.; Hung, W.-I.; Chou, H.-H.; Lin, J. T. *Org. Lett.* **2014**, *16*, 3052.
(22) Feng, Q.; Zhang, Q.; Lu, X.; Wang, H.; Zhou, G.; Wang, Z.-S. *ACS Appl. Mater. Interfaces* **2013**, *5*, 8982.
(23) Huang, Z.-S.; Cai, C.; Zang, X.-F.; Iqbal, Z.; Zeng, H.; Kuang, D.-B.; Wang, L.; Meier, H.; Cao, D. *J. Mater. Chem. A* **2015**, *3*, 1333.
(24) (a) Jiang, S.; Fan, S.; Lu, X.; Zhou, G.; Wang, Z.-S. *J. Mater. Chem. A* **2014**, *2*, 17153. (b) Ma, B.-B.; Peng, Y.-X.; Tao, T.; Huang, W. *Dalton Trans.* **2014**, *43*, 16601. (c) Ozawa, H.; Yamamoto, Y.; Kawaguchi, H.; Shimizu, R.; Arakawa, H. *ACS Appl. Mater. Interfaces* **2015**, *7*, 3152.

DOI: 10.1021/acs.joc.5b02590
J. Org. Chem. 2016, 81, 640−653

(d) Chu, B.; Wang, H.; Xerri, B.; Lee, K.-H.; Yang, T.; Wang, Z.; Lin, Z.; Liang, Y.; Adamo, C.; Yang, S.; Sun, J. *RSC Adv.* **2014**, *4*, 62472. (e) Liu, H.; Liao, X.; Li, X.; Wu, D.; Guo, Q.; Wu, J.; Qian, S.; Lan, J.; Wang, R.; You, J. *RSC Adv.* **2015**, *5*, 56865.

(25) (a) Zhou, L.; Jia, C.; Wan, Z.; Chen, X.; Yao, X. *Org. Electron.* **2013**, *14*, 1755. (b) Zhou, L.; Jia, C.; Wan, Z.; Li, Z.; Bai, J.; Zhang, L.; Zhang, L.; Yao, X. *Dyes Pigm.* **2012**, *95*, 743. (c) Huang, W.-K.; Cheng, C.-W.; Chang, S.-M.; Lee, Y.-P.; Diau, E. W.-G. *Chem. Commun.* **2010**, *46*, 8992. (d) Wang, Q.; Zhang, Z.; Zakeeruddin, S. M.; Grätzel, M. *J. Phys. Chem. C* **2008**, *112*, 7084.

(26) (a) Tsai, M.-S.; Hsu, Y.-C.; Lin, J. T.; Chen, H.-C.; Hsu, C.-P. *J. Phys. Chem. C* **2007**, *111*, 18785. (b) Kumar, D.; Justin Thomas, K. R.; Lee, C.-P.; Ho, K.-C. *Org. Lett.* **2011**, *13*, 2622. (c) Velusamy, M.; Hsu, Y.-C.; Lin, J. T.; Chang, C. W.; Hsu, C.-P. *Chem. - Asian J.* **2010**, *5*, 87. (d) Kumar, D.; Justin Thomas, K. R.; Lee, C.-P.; Ho, K.-C. *J. Org. Chem.* **2014**, *79*, 3159.

(27) Bodedla, G. B.; Justin Thomas, K. R. J.; Li, C.-T.; Ho, K.-C. *RSC Adv.* **2014**, *4*, 53588.

(28) (a) Inouchi, T.; Nakashima, T.; Toba, M.; Kawai, T. *Chem. - Asian J.* **2011**, *6*, 3020. (b) Inouchi, T.; Nakashima, T.; Kawai, T. *J. Phys. Chem. A* **2014**, *118*, 2591.

(29) Zhang, X.-H.; Kim, S. H.; Lee, I. S.; Gao, C. J.; Yang, S. I.; Ahn, K.-H. *Bull. Korean Chem. Soc.* **2007**, *28*, 1389.

(30) (a) Huang, W.-K.; Wu, H.-P.; Lin, P.-L.; Lee, Y.-P.; Diau, E. W.-G. *J. Phys. Chem. Lett.* **2012**, *3*, 1830.

(31) (a) Miyaura, N.; Yamada, K.; Suzuki, A. *Tetrahedron Lett.* **1979**, *20*, 3437. (b) Miyaura, N.; Suzuki, A. *Chem. Rev.* **1995**, *95*, 2457.

(32) Knoevenagel, E. *Ber. Dtsch. Chem. Ges.* **1896**, *29*, 172.

(33) Stille, J. K. *Angew. Chem., Int. Ed. Engl.* **1986**, *25*, 508.

(34) (a) Li, G.; Jiang, K.-J.; Li, Y.-F.; Li, S.-L.; Yang, L.-M. *J. Phys. Chem. C* **2008**, *112*, 11591. (b) Hara, K.; Sato, T.; Katoh, R.; Furube, A.; Ohga, Y.; Shinpo, A.; Suga, S.; Sayama, K.; Sugihara, H.; Arakawa, H. *J. Phys. Chem. B* **2003**, *107*, 597.

(35) Cheng, H. M.; Hsieh, W. F. *Energy Environ. Sci.* **2010**, *3*, 442.

(36) (a) van den Berg, O.; Jager, W. F. *J. Org. Chem.* **2006**, *71*, 2666. (b) Granzhan, A.; Ihmels, H.; Viola, G. *J. Am. Chem. Soc.* **2007**, *129*, 1254.

(37) Reichardt, C. *Chem. Rev.* **1994**, *94*, 2319.

(38) Nazeeruddin, M. K.; Zakeeruddin, S. M.; Humphry-Baker, R.; Jirousek, M.; Liska, P.; Vlachopoulos, N.; Ahklover, V.; Fischer, C. H.; Grätzel, M. *Inorg. Chem.* **1999**, *38*, 6298.

(39) Nazeeruddin, M. K.; Pechy, P.; Renouard, T.; Zakeeruddin, S. M.; Humphry-Baker, R.; Comte, P.; Liska, P.; Cevey, L.; Costa, E.; Shklover, V.; Spiccia, L.; Deacon, G. B.; Bignozzi, C. A.; Grätzel, M. *J. Am. Chem. Soc.* **2001**, *123*, 1613.

(40) (a) Hara, K.; Sato, T.; Katoh, R.; Furube, A.; Yoshihara, T.; Murai, M.; Kurashige, M.; Ito, S.; Shinpo, A.; Suga, S.; Arakawa, H. *Adv. Funct. Mater.* **2005**, *15*, 246. (b) Tian, H.; Sun, L. *J. Mater. Chem.* **2011**, *21*, 10592. (c) Hagfeldt, A.; Grätzel, M. *Chem. Rev.* **1995**, *95*, 49. (d) Grätzel, M. *Nature* **2001**, *414*, 338.

(41) (a) Kalyanasundaram, K.; Grätzel, M. *Coord. Chem. Rev.* **1998**, *177*, 347. (b) Green, A. N. M.; Palomares, E.; Haque, S. A.; Kroon, J. M.; Durrant, J. R. *J. Phys. Chem. B* **2005**, *109*, 12525.

(42) Parr, R. G.; Yang, W. T. *Annu. Rev. Phys. Chem.* **1995**, *46*, 701.

(43) Jiang, X.; Karlsson, K. M.; Gabrielsson, E.; Johansson, E. M. J.; Quintana, M.; Karlsson, M.; Sun, L.; Boschloo, G.; Hagfeldt, A. *Adv. Funct. Mater.* **2011**, *21*, 2944.

(44) (a) Lin, R. Y.-Y.; Chuang, T.-M.; Wu, F.-L.; Chen, P.-Y.; Chu, T.-C.; Ni, J.-S.; Fan, M.-S.; Lo, Y.-H.; Ho, K.-C.; Lin, J. T. *ChemSusChem* **2015**, *8*, 105. (b) Lin, R. Y.-Y.; Chu, T.-C.; Chen, P.-W.; Ni, J.-S.; Shih, P.-C.; Chen, Y.-C.; Ho, K.-C.; Lin, J. T. *ChemSusChem* **2014**, *7*, 2221.

(45) (a) Kuang, D.; Uchida, S.; Humphry-Baker, R.; Zakeeruddin, S. M.; Grätzel, M. *Angew. Chem., Int. Ed.* **2008**, *47*, 1923. (b) Fabregat-Santiago, F.; Bisquert, J.; Garcia-Belmonte, G.; Boschloo, G.; Hagfeldt, A. *Sol. Energy Mater. Sol. Cells* **2005**, *87*, 117. (c) Longo, C.; Nogueira, A. F.; De Paoli, M.-A.; Cachet, H. *J. Phys. Chem. B* **2002**, *106*, 5925. (d) Kern, R.; Sastrawan, R.; Ferber, J.; Stangl, R.; Luther, J. *Electrochim. Acta* **2002**, *47*, 4213.

(46) Wan, Z.; Jia, C.; Duan, Y.; Zhou, L.; Lin, Y.; Shi, Y. *J. Mater. Chem.* **2012**, *22*, 25140.

(47) Liu, L.; Hong, D.-J.; Lee, M. *Langmuir* **2009**, *25*, 5061.

DOI: 10.1021/acs.joc.5b02590
J. Org. Chem. 2016, 81, 640−653